LOW MAGNETIC SIGNATURE PROPULSION SYSTEM

D. Cope
Foster-Miller, Inc.
350 Second Avenue
Waltham, MA 02154-1196
617-684-4000

August 1996

· DISCLAIMER

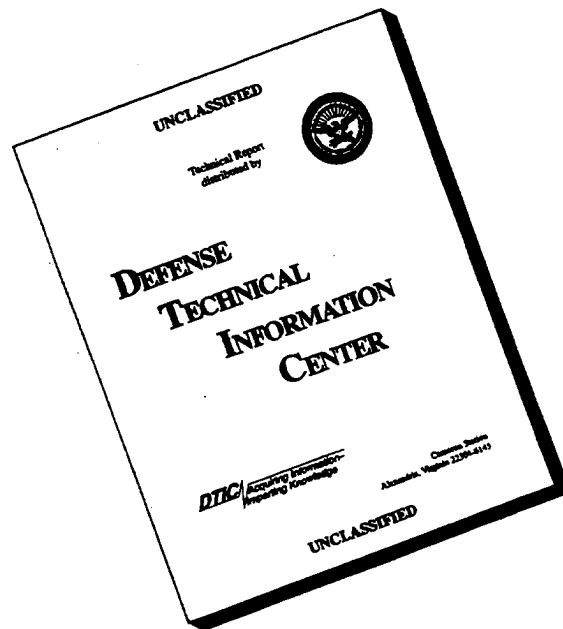**19960904 024**

Prepared for

U.S. Special Operations Command
7701 Tampa Point Boulevard
MacDill AFB, FL 33621-5323

DISCLAIMER NOTICE

UNCLASSIFIED

Technical Report
distributed by

**DEFENSE
TECHNICAL
INFORMATION
CENTER**

DTIC| Acquiring Information-
Imparting Knowledge

Cameron Station
Alexandria, Virginia 22304-6145

UNCLASSIFIED

THIS DOCUMENT IS BEST QUALITY AVAILABLE. THE COPY FURNISHED TO DTIC CONTAINED A SIGNIFICANT NUMBER OF PAGES WHICH DO NOT REPRODUCE LEGIBLY.

SOC-0057-FM-96025-1006

LOW MAGNETIC SIGNATURE PROPULSION SYSTEM

D. Cope
Foster-Miller, Inc.
350 Second Avenue
Waltham, MA 02154-1196
617-684-4000

August 1996

Final Technical Report
Contract No. USZA22-95-C-0057
Reporting Period: 27 November 1995 - 27 May 1996

DISCLAIMER

Prepared for

U.S. Special Operations Command
7701 Tampa Point Boulevard
MacDill AFB, FL 33621-5323

REPORT DOCUMENTATION PAGE

Form Approved
OMB No. 0704-0188

1. AGENCY USE ONLY *(Leave blank)*	2. REPORT DATE August 1996	3. REPORT TYPE AND DATES COVERED Final Technical Report Period Covered: 27 November 1995-27 May 1996	
4. TITLE AND SUBTITLE Low Magnetic Signature Propulsion System		5. FUNDING NUMBERS 1SD300-5150-0100	
6. AUTHOR(S) D. Cope			
7. PERFORMING ORGANIZATION NAME(S) AND ADDRESS(ES) Foster-Miller, Inc. 350 Second Avenue Waltham, MA 02154-1196		8. PERFORMING ORGANIZATION REPORT NUMBER SOC-0057-FM-96025-1006	
9. SPONSORING/MONITORING AGENCY NAME(S) AND ADDRESS(ES) U.S. Special Opertons Command 7701 Tampa Point Boulevard MacDill AFB, FL 33621-5323		10. SPONSORING/MONITORING AGENCY REPORT NUMBER USZA22-95-C-0057	
11. SUPPLEMENTARY NOTES TPO: Mr. Wattenbarger			
12a. DISTRIBUTION/AVAILABILITY STATEMENT "Nothwithstanding any other legends marked hereon, this document contains information which may disclose a patentable invention in which the Government has a right, title or interest. Further distribution of this document to any non-governmental agency is prohibited without written approval of USSOCOM/SOKO."		12b. DISTRIBUTION CODE N/A	

13. ABSTRACT *(Maximum 200 words)*

The electric propulsion system of the SEAL Delivery Vehicle (SDV) has associated magnetic fields whether operating or not. These fields were measured and documented and the feasibility of a magnetic shielding system was proven during this program. The shielding system was demonstrated on a surrogate electric motor in Foster-Miller's laboratory and by computer simulation of the battery pack. The substitute motor and battery pack simulation were used due to limited availability of the SDV for actual shield installation and validation.

The major magnetic field sources of the SDV were: the battery pack, the ferromagnetic motor mass and the operating motor itself. Detection ranges were calculated for each major field source of the SDV and varied depending upon motor load. Actual detection ranges may be greater or lesser depending upon the actual operating conditions, detection threshold sensitivity, and the ambient magnetic noise environment.

The shielding system consisted of active magnetic field cancellation for the ferromagnetic motor mass and simulated conductor re-routing for the battery pack. The results of the magnetic signature reduction were: motor field reduced by 21 dB and the battery pack field reduced by 15 dB. This level of magnetic field reduction decreased the calculated detection ranges by 55 percent.

14. SUBJECT TERMS magnetic anomaly, magnetic signature reduction, active magnetic shielding			15. NUMBER OF PAGES 66
			16. PRICE CODE N/A
17. SECURITY CLASSIFICATION OF REPORT Unclassified	18. SECURITY CLASSIFICATION OF THIS PAGE Unclassified	19. SECURITY CLASSIFICATION OF ABSTRACT Unclassified	20. LIMITATION OF ABSTRACT Unlimited

NSN 7540-01-280-5500

Standard Form 298 (Rev. 2-89)
Prescribed by ANSI Std. 239-18

CONTENTS

ILLUSTRATIONS

1. EXECUTIVE SUMMARY

SEAL Delivery Vehicles (SDVs) and larger underwater platforms are force enhancers as they significantly increased diver mobility and effectiveness while reducing fatigue. These vehicles need powerplants with low magnetic signatures for minefield stealth; minimum interference with navigational, search and other equipment; and operator safety and comfort.

The most serious threat to both commercial shipping and amphibious military operations is the magnetic naval mine due to the ubiquitous nature of magnetically permeable materials in and around vessels which inadvertently increase the effective range of the mine. The increasing sophistication of the magnetic mine threat invalidates piecemeal solutions. The threat is becoming smarter and so must we.

The propulsion system for the SDV consists of electric motors, controllers, and batteries and distribution conductors. Magnetic fields emitted from these components pose a serious threat of magnetic mine activation. In addition, these fields interfere with navigation and magnetic search missions and raise operational safety and comfort issues. Also magnetic emissions provide observable (and therefore undesirable) signature components and reduce the overall system stealth.

Significant sources of magnetic field are the battery, current in the distribution conductors, the electric motor, and, to some extent, the motor controller. A magnetic field signature is created by all electric motors, controllers, distribution conductors and battery types, although certain types of each component inherently produce a greater or lesser signature than other types.

Experience has shown that the magnetic signature of electric motors changes non-linearly with load. In fact, as discussed below, the signature can be divided into load-dependent and load independent components. Therefore, a passive signature reduction system will be inadequate at reducing the motor emission at all loads and an active approach must be taken. Active shielding can be defined as the determination and application of currents which exactly cancel the magnetic field anomaly of an arbitrary body, such as a ferromagnetic body with currents.

It is noteworthy that the magnetic field due to battery current distribution is linear with increasing current and passive shielding of this particular component is possible. The rate of decay in amplitude of the magnetic field with increasing distance from the vehicle depends significantly upon the conductor geometrical distribution.

Major Accomplishments

The following are the major accomplishments under this program.

* Magnetic measurements made of an SDV.
* Component analysis of the source magnetic fields.
* Prediction of detection ranges (unshielded).
* Two battery pack configurations shielded numerically.

1

- Demonstrated motor active shielding (substitute motor).
- Retrofit battery pack signature reduction of 15 dB.
- Demonstrated motor signature reduction of 21 dB (substitute motor).

Significant magnetic signature reduction of the SDV electric propulsion system has been demonstrated, 15 to 21 dB depending upon the component under consideration. Due to limited availability of the vehicle, signature reduction was demonstrated on substitute components or numerically simulated.

Existing SDVs (and other platforms) can be retrofitted with an advanced shielding system and experience a significant reduction in magnetic field signature. Based upon our experience and initial estimates, a magnetic signature reduction of greater than 20 dB is probable by retrofitting a signature reduction system.

Future design SDVs (and other platforms) can benefit from even greater signature reductions. Although the actual levels achieved will depend upon the details of the vehicle design, suppression levels could be 26 dB or more compared to present levels.

2

2. INTRODUCTION

2.1 Purpose of the Program

The electric propulsion system of the Seal Delivery Vehicle (SDV) has associated magnetic fields, whether it is operating or not. These fields were measured and documented and the feasibility of a shielding system was proven with this program. Based upon the measurements, SDV magnetic detection ranges were predicted. The shielding system was demonstrated on a surrogate electric motor in Foster-Miller's laboratory and by computer simulation of the battery pack. The substitute motor and battery pack simulation were used due to limited availability of the SDV for actual shield installation and validation.

The major measured magnetic field sources of the SDV were: the battery pack, the ferromagnetic mass of the motor and the operating motor itself. The detection ranges were calculated for each major field source of the SDV. The computed detection ranges varied from 46 ft (14m) for an unloaded motor to 55 ft (16.7m) with a 50A motor load. The peak current load is approximately 100A. It is important to note that the detection distances were calculated based upon field measurements during no-load operation of the SDV and the actual detection ranges may be greater or lesser depending upon the actual operating conditions, detection threshold sensitivity, and the ambient magnetic noise environment.

The shielding system consisted of active magnetic field cancellation for the ferromagnetic motor mass and simulated conductor re-routing for the battery pack. The results of the magnetic signature reduction were: motor field reduced by 21 dB and the battery pack current field reduced by 15 dB. This level of magnetic field reduction decreased the calculated detection ranges by 55 percent to 20.4 ft (6.2m) and 25.4 ft (7.75m), respectively. A greater field reduction is possible with additional effort resulting in a further decrease of the detection ranges.

2.2 Application Description

Seal Delivery Vehicles (SDVs) and larger underwater platforms are force enhancers as they significantly increased diver mobility and effectiveness while reducing fatigue. These vehicles need powerplants with low magnetic signatures for minefield stealth; minimum interference with navigational, search and other equipment; and operator safety and comfort.

Electromagnetic shielding is a systems issue. The most effective countermeasure to magnetic mines is to physically destroy the mines by any of a variety of means of hard target killers. Implementing these means can be accomplished by divers, but the signature of the divers and their associated systems must be suppressed to below the mine triggering threshold.

Experience has shown that the magnetic signature of electric motors changes non-linearly with load. Therefore, a passive signature reduction system will be inadequate at reducing the motor emission at all loads and an active approach must be considered. The magnetic field due to battery current distribution, however, is linear with current and therefore passive shielding is possible.

Magnetic signature management must be real-time, adaptive, and flexible. A systems viewpoint has been taken since it ensures that the signature suppression approach properly balances signature reduction benefits with overall system resources including added system weight, volume, power requirements, capital and operating costs.

Active shielding can be defined as the determination and application of currents which exactly cancel the original magnetic field of an arbitrary body, such as a ferromagnetic motor with currents. Active shielding was demonstrated on a surrogate electric propulsion system of the SDV. Advanced modeling and control techniques were used to design an adaptive, flexible system which provides significant reduction in magnetic emissions.

Throughout this document, when several sources of magnetic field are discussed even though one may appear to be dominant, it is the balanced system approach which is evident. As a single source signature is reduced, other sources become relatively more important. The best overall signature reduction system was pursued from a complete system perspective. This ensured that an approach was taken which balanced the signature reduction benefit against the inevitable tradeoff be it weight, volume, power requirement, capital or operating costs. Shielding system growth capabilities must also fit into the systems perspective.

2.3   Conclusions

The magnetic field of the SDV was measured and documented under no-load conditions. Based upon these measurements, detection ranges were calculated based upon no-load (1A) and substantial-load (50A) conditions. The unshielded minimum (no-load) detection range was approximately 46 ft (14m). A magnetic signature reduction system was devised which consisted of an active shield for the ferromagnetic motor and conductor re-wiring for the battery pack. The shielding system reduced the detection ranges by 55 percent to approximately 20 ft (6.2m). An additional reduction in detection range is possible with improved shielding.

2.4   Summary

The magnetic field of the SDV has been measured and documented under motor no-load conditions. The field exhibits characteristic signature traits which permits detection at distances up to 46 ft (14m) even when it is not operating. When the motor is operating and loaded the detection range is estimated to increase to 55 ft (16.7m).

A magnetic shielding system was devised based on a substitute motor and a simulated battery pack. The shielding system reduced the emitted magnetic field by 21 dB resulting in a reduction of the detection range by 55 percent to a minimum of 20.4 ft (6.2m). Substitute components were used instead of the actual components due to limited availability of the SDV. As noted in the text, additional reduction in magnetic field and detection range is possible with additional effort.

The basic methodology employed in this effort was: measurement of the magnetic fields of the SDV, analysis of the data, design and fabrication of a shielding system, and validation testing to prove the shield effectiveness. This methodology has been used previously for magnetic field signature reduction for applications as diverse as: ac and dc motors, battery packs, solenoid-driven circuit breakers, superconducting Maglev high speed trains, the interior and exterior of automotive electric vehicles, and automotive internal combustion engines. The methodology will be used on future projects due to its logical progression of understanding of the fields and successful signature reduction results. The fundamental methodology can also be used on other applications, including acoustic signature reduction.

4

3. APPARATUS AND EQUIPMENT

This section describes the major apparatus and equipment that has been procured, fabricated, modified, or otherwise used in this study. In general, the following subsections describe all major areas of effort. The first subsection describes the SDV battery pack, including both known configurations. The next two subsections briefly describe the SDV permanent magnet and the laboratory induction motors. The motors are generally in the same horsepower class. The next two subsections describe the equipment used to acquire data concerning the magnetic field and applied currents. The final subsection summarizes the apparatus and equipment investigated.

3.1 SDV Battery Pack Description

The electric motor used for propulsion of the SDV is power by approximately 20 batteries. These batteries are arranged in three and one-third (3-1/3) trays of six batteries in each tray. Each battery is composed of five cells of voltage 1.5V. Thus, each battery is 7.5V, each tray is 45V and the total propulsion system is 150V nominal. The remaining two-thirds of the fourth tray are used for other electrical needs (so-called "hotel power").

The current supplied by these batteries is a significant source of the emitted magnetic field. This magnetic field can be reduced through proper routing of the cables in order to reduce the magnetic dipole moment of the electric current distribution.

The wiring of the SDV batteries is accomplished using two different configurations. The first configuration (herein labeled the "original") is presented in Figure 1 and shown
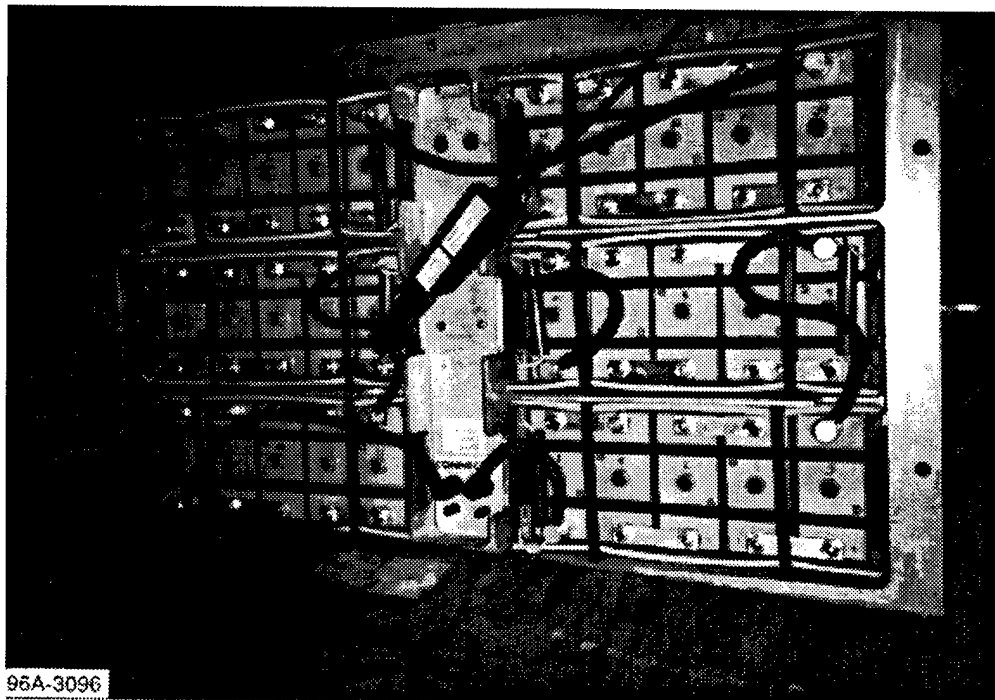
Figure 1. *Photograph of original battery pack configuration (with current probe)*

5

schematically in Figure 2. Note, these schematics are drawn to resemble the actual electric cabling as closely as possible. It is our understanding that this configuration is still in use for one tray in the prototype SDV, but will be changed for subsequent vehicles for reasons of installation simplicity.

For ease and repeatability of cable attachment by the operators, a different configuration was redesigned into the "present" battery configuration. The present battery tray configuration is shown in Figure 3 and presented schematically in Figure 4.

In the above figures, it can be seen how the electric cabling encloses a finite area during its routing through the batteries. As discussed below, this finite area gives rise to a magnetic dipole moment creating magnetic fields at a distance from the SDV.

3.2 SDV Motor Description

The SDV motor used for propulsion is a specifically-designed 32 pole permanent magnet motor. The motor has a cylindrical shape with a radius of about 9 in. and a length of about 12 in. Of particular note is the additional backiron used in the motor design. This was done to increase motor efficiency and to reduce the stray emitted field due to operation of the motor. Unfortunately, this backiron contributes to the ferromagnetic mass of the motor. The magnetic effect of ferromagnetic material in the earth's ambient magnetic field is discussed below. The motor is rated at 10 hp, but is capable of producing power substantially beyond ratings.

Figure 2. **"Original" battery tray configuration**

3.3 Laboratory Motor

Because the SDV is actively undergoing technical development, there was limited hands-on access to the SDV motor. For purposes of demonstrating magnetic shielding a substitute laboratory motor was used. This motor was a commercially available 7.5 hp three-phase induction motor with an active stack radius of 4.8 in. and a length of 11.0 in.

Ideally, for best correlation between laboratory and field practice, the motor used in the shielding demonstration would have been very similar to the SDV motor. This was not possible within the constraints of the program. The justification for use of an induction motor was:

- An induction motor of similar horsepower rating was available within our laboratory.

- The most significant measured magnetic signature was due to the ferromagnetic mass. Therefore, the main magnetic effect of the SDV motor was replicated without operating the motor. A photograph of the laboratory motor is presented in Figure 5.

6

96A-3097

Figure 3. **Photograph of present battery pack configuration**

In Figure 5, note how the three coils are wound around the center of the motor in a tight spool. The magnetic signature reduction achieved (21 dB) demonstrated feasibility of the shielding approach.

3.4 Data Acquisition System

The data acquisition system consisted of a 75 MHz Intel 80486 Toshiba portable computer with 8 MB of RAM and 522 MB of hard disk space. The purpose of the data acquisition system was to acquire, digitize, and store the results of the data measurements. The data was analyzed by the methods discussed below.

The data acquisition card used in the computer was a UEI WIN-30DS board with a throughput of 1 MHz and an input signal dynamic range of ±5V. The board has 12 bits which gave a raw resolution of 2.5 mV. To facilitate recording of low levels of magnetic field, a three-channel amplifier was built with a selectable gain switch of 1X, 20X, and 200X. Custom circuitry was installed to protect the board input channels from overvoltages from unconditioned input signals. Up to 16 channels of data (12 of which are buffered) can be simultaneously acquired with this equipment.

3.5 Sensors

This subsection details the sensors used to measure the relevant characteristic properties of the SDV. The sensors used were magnetometers, current probes, and string pots.

7

3.5.1 Magnetometers

The magnetometers used to measure the magnetic signature of the circuit breaker were Bartington MAG-03MC three-axis fluxgate magnetometers. Two versions were used depending on sensitivity requirements, 500 µT and 100 µT, with sensitivities of 5 nT and 1 nT respectively. The units have a bandwidth from 0 Hz (dc) to 1.5 kHz. A high pass filter could be used to cut off frequencies of 0.1 Hz and below. This eliminated the earth's background field from the measurement. The bandwidth for AC measurements was 1.5 kHz.

3.5.2 Current Probes

Four brands of current probes were used to measure various currents associated with the operation of the circuit breaker. Important characteristics of the probes are given in Table 1.

3.5.3 String Pot

A string "pot" (or, more formally, variable resistance potentiometer) is a device which outputs a voltage proportional to the distance the transducer is moved. The magnetic field anomaly generated by the ferromagnetic mass within the earth's field can be measured by holding the mass stationary and moving a magnetic field probe past the mass. A fixed voltage is applied across the string pot and

Figure 4. **"Present" battery tray configuration**

the output (signal) voltage varies with the position of the endpoint of the string. Thus, magnetic field can be correlated to the geometry of the ferromagnetic mass simply by noting the pull path with respect to the mass.

A field failure of a string pot occurred due to shipping. This prevented accurate distance measurements from being made during the COASTSYSSTA visit. At the time of the measurements, it was necessary that consistent steady velocity timing pulls be executed by the operator to approximate a field-versus-distance plot by a field-versus-time plot. After several calibration tests it was decided that the operator was fairly consistent and the data, while imprecise, would suffice for the feasibility study. Some of the magnetic field plots below are plotted as a function of time. It will be seen that over a pull period of six (6) seconds the plots are quite reproducible, indeed.

The failure of the string pot was identified and repaired at our facility after which the string pot performed flawlessly. The string pot was important to the laboratory measurements since it allowed more precise comparison to be made of different magnetic field "pulls."

Figure 5. *Induction motor used in laboratory demonstration (shown with cancellation coils)*

Table 1. Current probes

Model	Tektronix A622	Fluke Y8100	LEM PR-30	A.W. Sperry DSA-2009
Maximum Current	100A	20A or 200A	30A	200A or 2000A
Output	100 mV/A	100 mV/A or 10 mV/A	100 mV/A	1 mV/A or 0.1 mV/A
Bandwidth	0 to 100 kHz	0 to 20 kHz	0 to 100 kHz	0 to 2000 Hz
Sensitivity	10 mA	10 mA	10mA	1 A

3.6   Summary

The apparatus and equipment used in this program were briefly described in this section. The SDV apparatus which generated the magnetic field signature consists mainly of the battery pack and motor. The substitute laboratory motor was also described since the shielding was actually demonstrated on it.

A highly capable suite of sensors and computer data acquisition system was assembled to measure the magnetic fields, currents, and distances associated with the SDV. This equipment was briefly described.

In summary, the sources of magnetic field and the means for detecting it were identified and characterized. This information establishes the basis for the generated magnetic fields and the accompanying magnetic signature reduction.

4. MAGNETIC MEASUREMENTS

In order to demonstrate the effectiveness of the magnetic signature reduction system using active cancellation, a prototype system was designed, fabricated, and tested on the laboratory motor. This section describes the SDV measurements made at COASTSYSSTA, Panama City, FL and laboratory measurements made at Foster-Miller's facility in Waltham, MA.

4.1 SDV Magnetic Measurements

Magnetic field measurements were made of the SDV at COASTSYSSTA on 16 January, 1996. The measurements were conducted within a building which significantly affected the results, as discussed below. Three main magnetic field sources were identified as a result of these measurements. These sources are: ferromagnetic masses, motor operation, and battery currents.

It was intended to return to the COASTSYSSTA for further measurements encompassing both source and shielded component investigations. Unfortunately, due to the SDV schedule this was not possible.

4.1.1 SDV Ferromagnetic Mass Magnetic Anomaly Measurements

As discussed above, the SDV motor was constructed with extra backiron to reduce the permanent magnet signature. However, due to the quantity of backiron in the motor used, there is a significant magnetic anomaly associated with this motor when it is placed within an otherwise uniform magnetic field such as the earth's field. This magnetic anomaly represents a distinctive signature which was experimentally characterized through magnetic field measurement and analysis.

These tests consisted of pulling a three-axis magnetometer past the electric motor while recording the magnetic field components in the three Cartesian directions. By measuring and calculating the perturbations to the earth's ambient magnetic field, the amplitude of the magnetic anomaly can be quantified.

Figure 6 presents the magnetic field components measured by the magnetometer array as it passes by the SDV.

As can be seen in Figure 6, the presence of the backiron in the electric motor yields a distinctive magnetic signature that can be detected using simple magnetic field sensors.

By analyzing the data presented in Figure 6, the magnetic moment of the SDV electric motor can be determined. As shown in Figure 6, the maximum perturbation component is measured to be 0.59V (= 59 mG) measured at a distance of about 0.7m. By using the analysis presented below, this yields a magnetic moment equal to about 12 A-m^2. This is slightly more than the predicted magnetic moment of the SDV motor based on motor volume which is equal to 4 A-m^2. The difference between the predicted magnetic moment and the experimentally observed magnetic moment can be attributed to additional ferromagnetic material used to brace the electric motor in addition to motor housing.

10
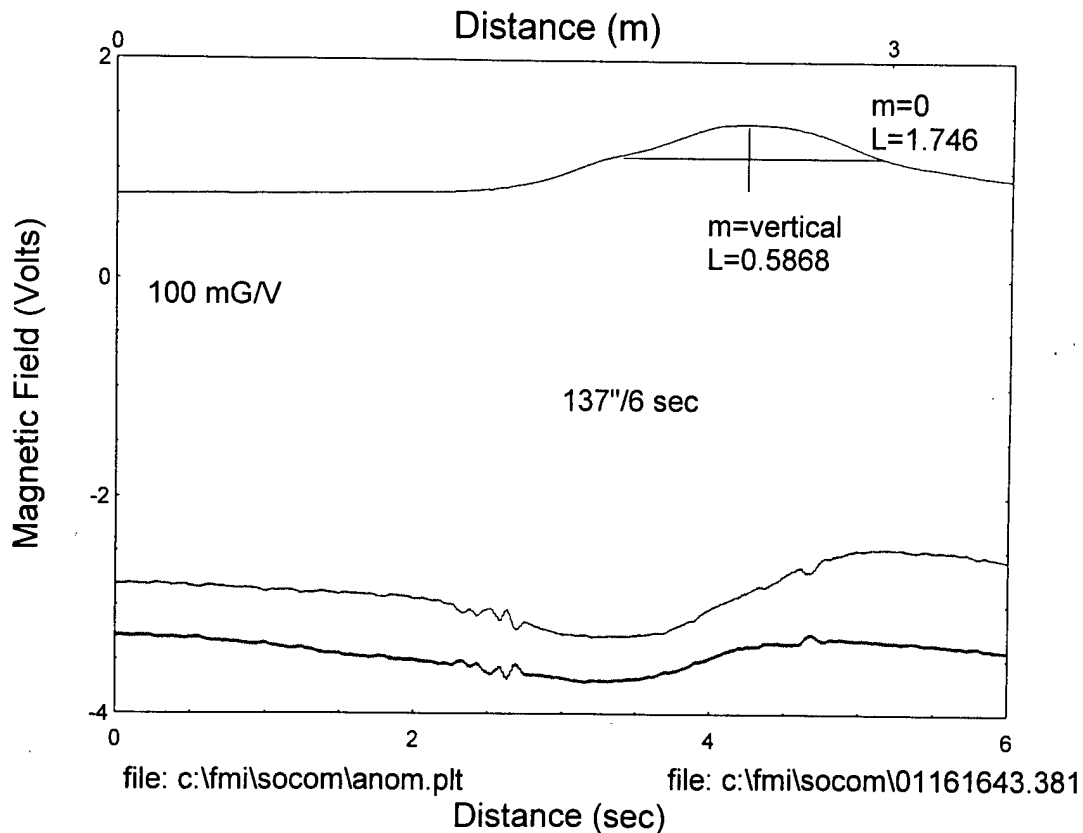
Figure 6. *Magnetic perturbations due to backiron in SDV motor*

In conclusion, measurement of the magnetic anomaly of the SDV electric motor permits approximate determination of the size and location of the motor. This is, of course, extremely detrimental to stealthy operation of the vehicle.

4.1.2 SDV Motor Operation Measurements

The magnetic characteristics of the SDV electric motor were determined during motor operation. There were three operating modes during which the SDV motor magnetic characteristics were determined:

- Off (no energization at all).
- Standby (control electronics energized but motor not turning).
- On (control electronics energized and motor turning).

Magnetic characteristics were determined using a three-axis magnetometer swept past the motor. During the passage of this array, the three Cartesian components were measured and recorded as a function of distance.

After recording the above data, significant changes in the z component of the magnetic field were observed. Figure 7 presents the z component of the magnetic field as a function of time as the magnetometer was swept past the motor.

(Note that the field is plotted against time. As discussed previously, this was because the string pot was damaged during shipping and it was necessary for the operator to simply pull the magnetometer at a consistent steady velocity. The relatively small variation in time of peak suggests the operator was remarkably consistent indeed.)

11
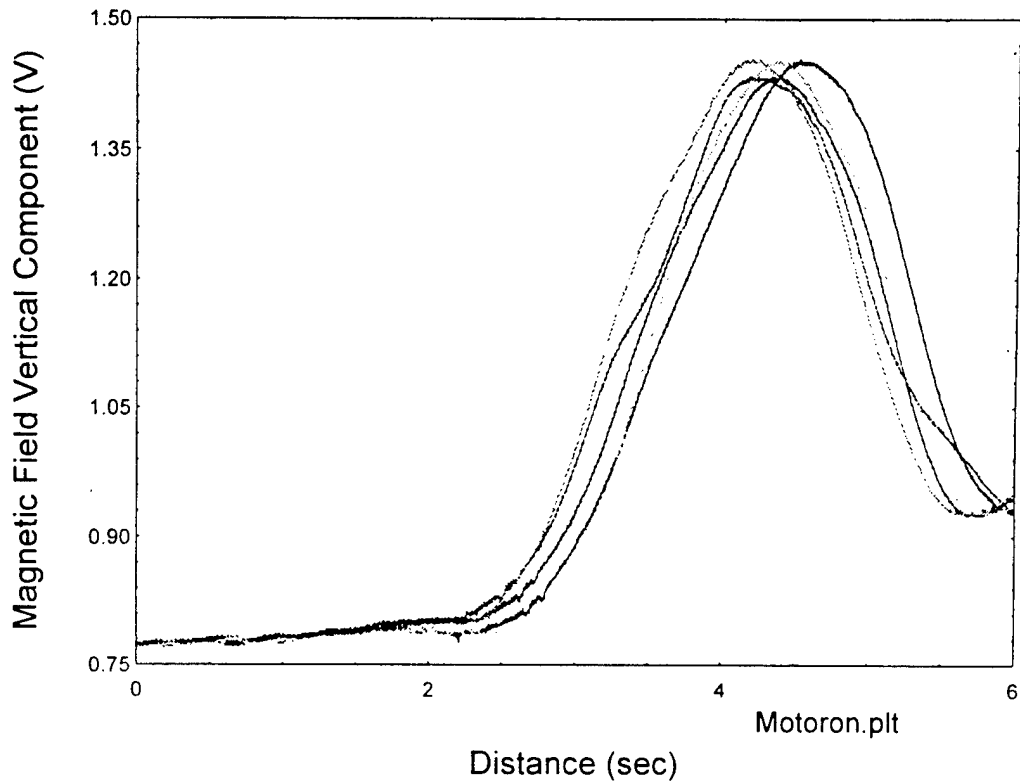
Figure 7. *SDV motor magnetic fields in off, standby, and on modes*

Although difficult to see at full scale, the z component of these magnetic fields show differences in their peak value depending on the motor operating mode. Figure 8 presents a close-up view of the peak magnetic fields presented in Figure 7 with the operating mode identified.

In Figure 8, it can be seen that the peak magnetic field with the motor "Off" reaches a level of 1.43V. With the Motor "On" as well as in "Standby" mode, the peak field reaches a level of 1.45V. This corresponds to a magnetic field difference of 2 mG. While this difference is small, it is clearly observable and repeatable. It should be remembered that this data was taken with a motor current of only about 1A. The low current value was due to the no-load operation of the motor.

In the future, up to a full load should be put on the motor to measure the stray magnetic field under all conditions. It is not known how the field varies according to load or current. Therefore, in the analyses below two bounding cases are assumed: the magnetic field does not change with current and the field is linearly proportional to current. With an operating current of 50A, the magnetic signature could potentially increase to 0.1G measured at the 0.7m distance.

The magnetic field dependence on the current level in the SDV motor needs further study in order to prove or disprove the assumed linear scaling. This would require magnetic field studies under higher operating currents than were allowable in the present configuration (without a load).

12
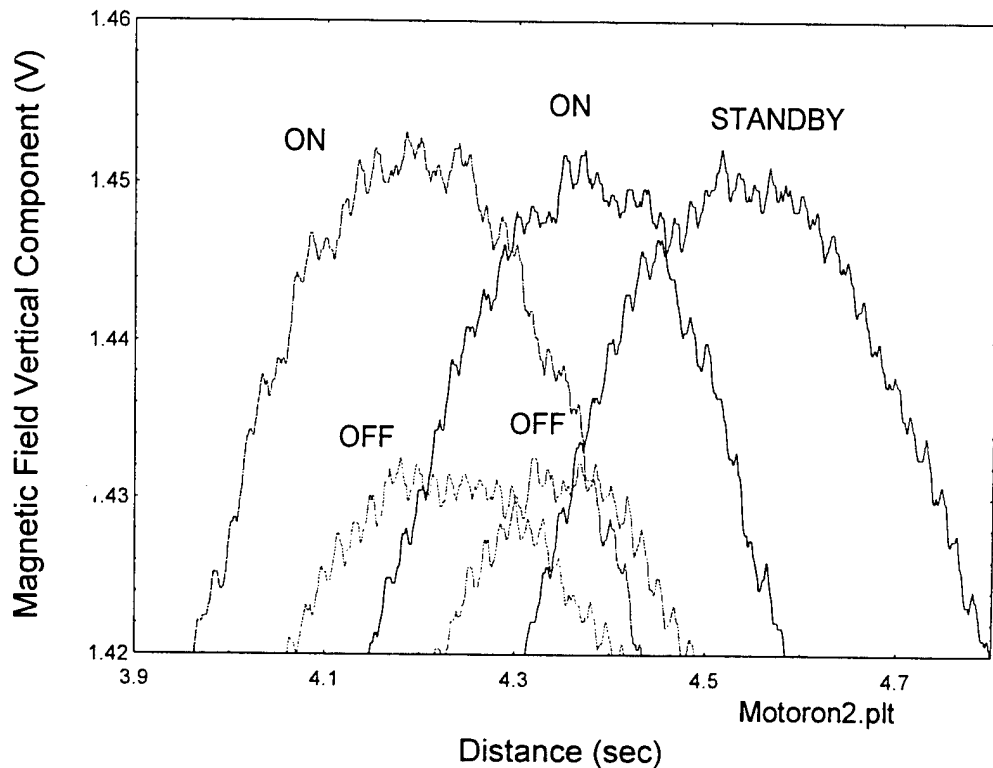
Figure 8. *Close-up of SDV motor fields*

4.1.3 SDV Battery Pack Magnetic Anomaly Measurements

The magnetic field associated with the SDV electric currents was measured with the motor in the Off, Standby, and On modes. Due to the low currents involved in operating the motor no-load, however, the magnetic fields were not observable above the building background using available test equipment. As discussed later, the estimated emitted magnetic field associated with the 1A current would be equal to 20 nT. As a coincidence, this is equal to the equipment's measurement resolution of 20 nT when configured as for the COASTSYSSTA trip. The equipment can actually detect fields of much smaller values when properly configured.

It should be noted that with the increased currents (50A) utilized under normal motor loads this magnetic field would be increased by a factor of 50 times. Theoretical and numerical models of the battery pack stray magnetic fields estimated the field to be readily detectable at significant distances when supplying load currents from 10A and greater. Therefore, shielding the battery pack was demonstrated using a 3-D magnetic field analysis software package. As noted above, two battery pack configurations were analyzed and shielded.

The magnetic field near the battery pack was measured and analyzed for frequency content. Figure 9 shows the Fourier transform of the measured magnetic field of the SDV during a transverse motor pull. The data clearly shows significant frequency structure at 60 Hz, 180 Hz, 300 Hz, and 420 Hz and little else. These frequencies correspond to the fundamental and odd-harmonics of the utility power system (1st, 3rd, 5th, and 7th harmonics).

The fact that these frequencies dominate the field measurements simply indicates that the greatest field source within the building where the measurements took place had these characteristics. One likely explanation is that as a result of the ubiquitous nature of the utility

13
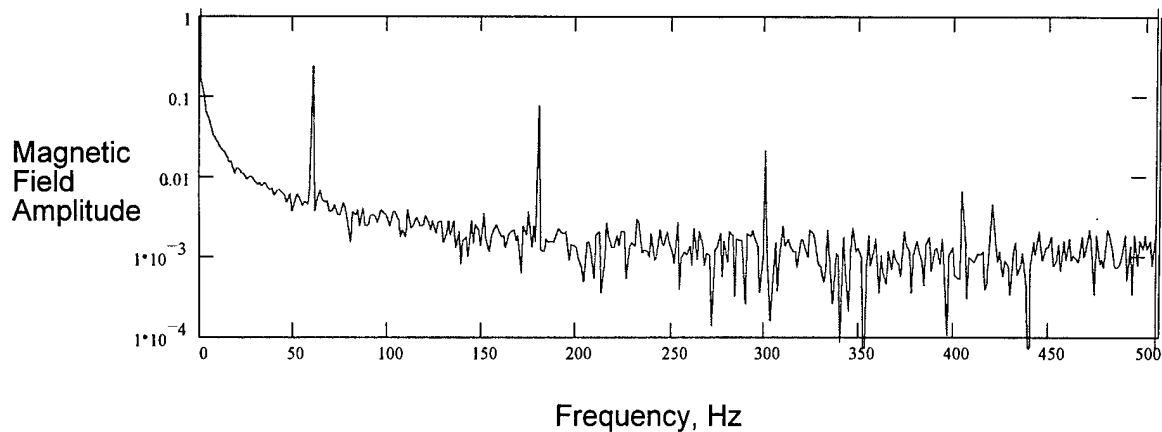
Figure 9. FFT of measured magnetic field (run mode)

frequency, fields of that frequency and its harmonics are wherever buildings and electric power are located. A second explanation for the lack of a characteristic SDV magnetic field signature within the measured field is the low amplitude battery current used for the measurements.

The battery current was also analyzed for frequency content. Figure 10 shows the fast Fourier transform of the measured SDV battery current waveform while in Run mode and OFF mode. The data clearly shows structure to the current waveform.

This data, in combination with numerical calculations of the effect of greater load currents, indicates that there will be an identifiable magnetic signature during operation of the SDV. When the current is sufficiently small (I~1A — as measured), the signature will be small. When the current is larger (I~50 to 100A) the magnetic field signature will be 50 to 100X greater and uniquely identifiable.
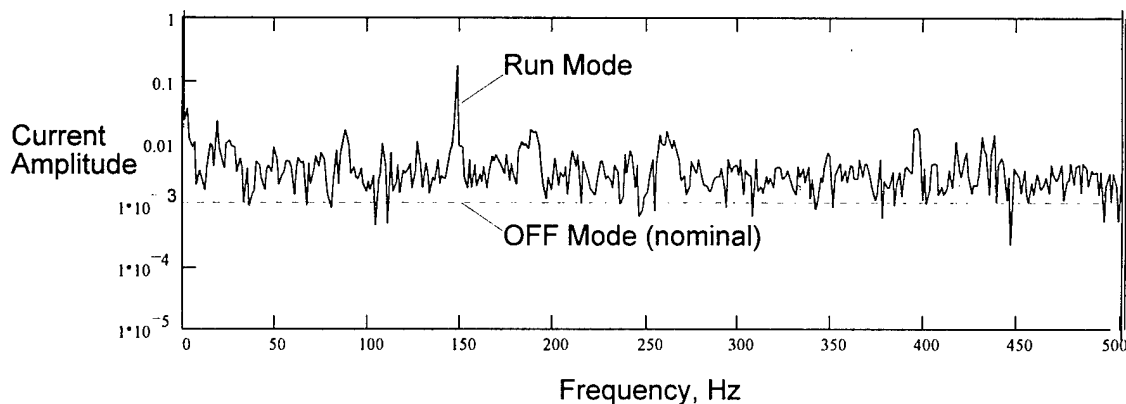
Figure 10. FFT of measured current trace

14

This conclusion is based upon the calculated linear proportionality between the battery current and the emitted stray magnetic field. Although the high background noise environment of the building, combined with the low no-load current of the motor, did not permit measurement of the magnetic field of the no-load battery current, the signature of the current waveform clearly indicates that under realistic operating conditions a magnetic field signature will be observable.

4.2   Laboratory Experiments

This subsection describes the experiments performed on the induction motor to measure and predict the emitted magnetic field. The shielding demonstration consisted of measuring and recording the magnetic field under three conditions:

1. The no-motor field of our laboratory.

2. The anomaly field in the presence of the motor (before shielding).

3. The field in the presence of the motor after activating the magnetic shield. This condition is discussed in more detail in a later section.

The anomaly to the ambient magnetic field due to the presence of a 7.5 hp induction motor can be obtained by the difference of the field in the presence of the motor and the no-motor field [(2) - (1)].

In order to demonstrate the effectiveness of the magnetic signature reduction system, the ambient magnetic field was measured in the absence of the motor. Figure 11 presents the three measured Cartesian components (x, y, z) of the magnetic field (as labeled) as a function of distance.
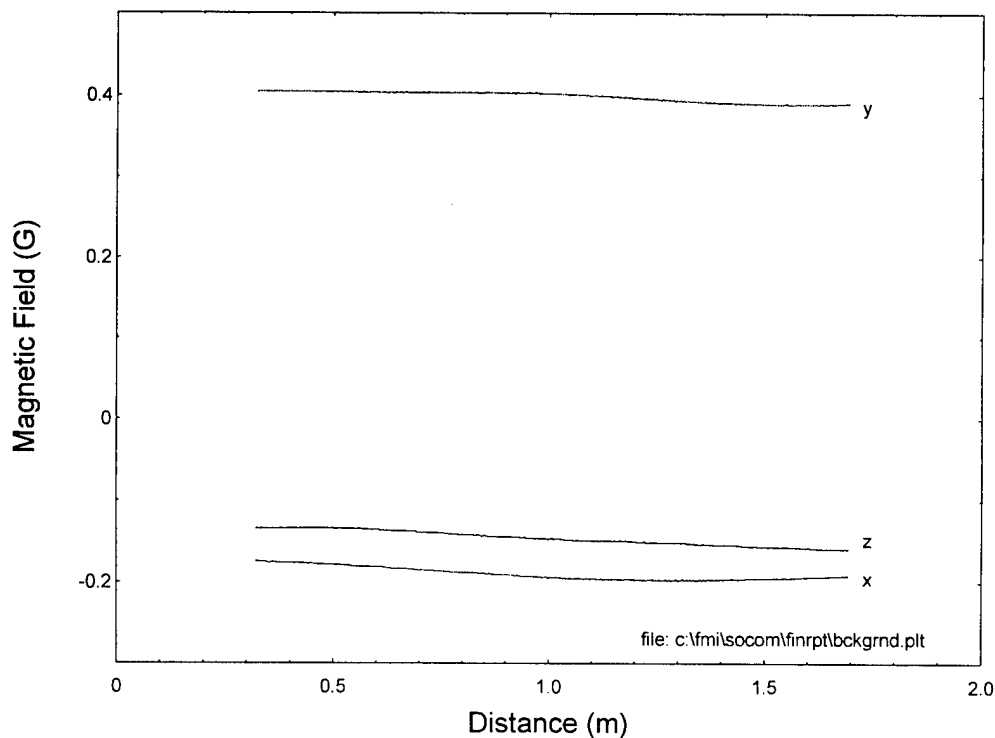
Figure 11.   Measured ambient magnetic field in laboratory

15

In Figure 11, the slight variation in field measured over this distance is due to the presence of steel structures in the walls of the laboratory. This effect is similar to the background perturbations which would be present in the presence of geological magnetic anomalies in the vicinity of the SDV.

The motor was placed in this environment (no shield) and the magnetic field levels were again measured the results presented in Figure 12 were obtained. Again, the three Cartesian magnetic field components are graphed as a function of distance. (Note this plot is similar to the SDV motor field versus time plot exhibited above.)

When these magnetic field levels are examined one at a time, the vertical scale for each field component can expanded as shown in Figure 13. When the ambient magnetic field is subtracted from these measurements, the results presented in Figure 14 are obtained. Figure 14 presents the magnetic field perturbations (all three Cartesian components) as a function of distance. The apparent increase in noise presented in Figure 14 is a result of the magnification of the vertical axis (since the baseline offset due to earth's field has been subtracted). This graph shows the perturbation to the ambient field due to the ferromagnetic mass of the motor. As can be deduced from the figure, the sensor array passed almost directly below the magnetic anomaly of the electric motor.

The data presented in Figure 14 demonstrates the characteristic dipole signature of the magnetic perturbation. This is the magnetic signature that must be canceled even when the motor is Off. This signature depends upon the earth's ambient magnetic field direction. Therefore, for example, as the vehicle changes heading the active shielding coils must change to compensate.
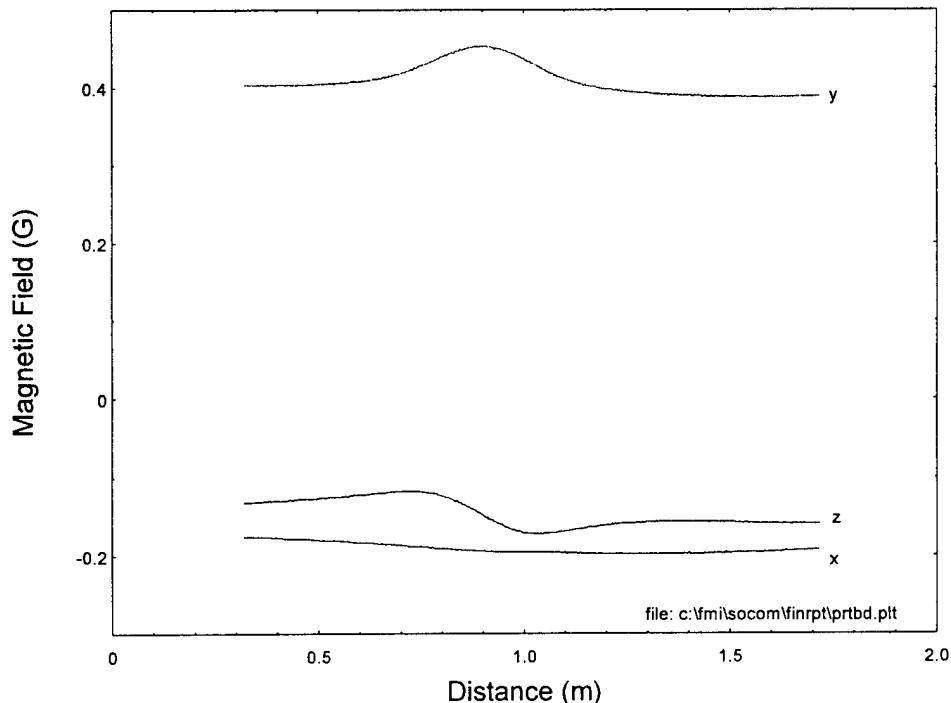
Figure 12. Measured magnetic field components in presence of motor

16
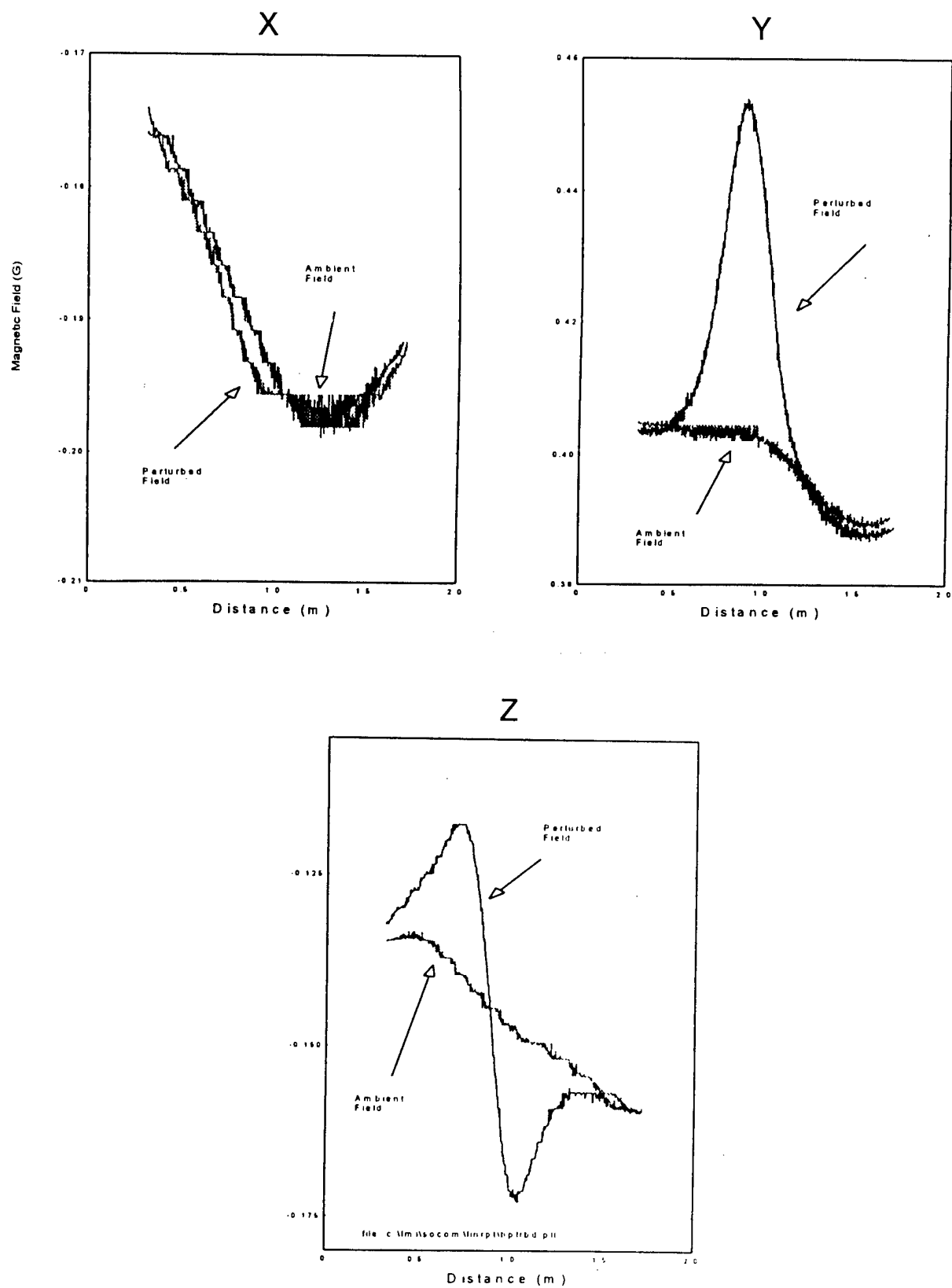
Figure 13. Close-up of magnetic field components in presence of motor
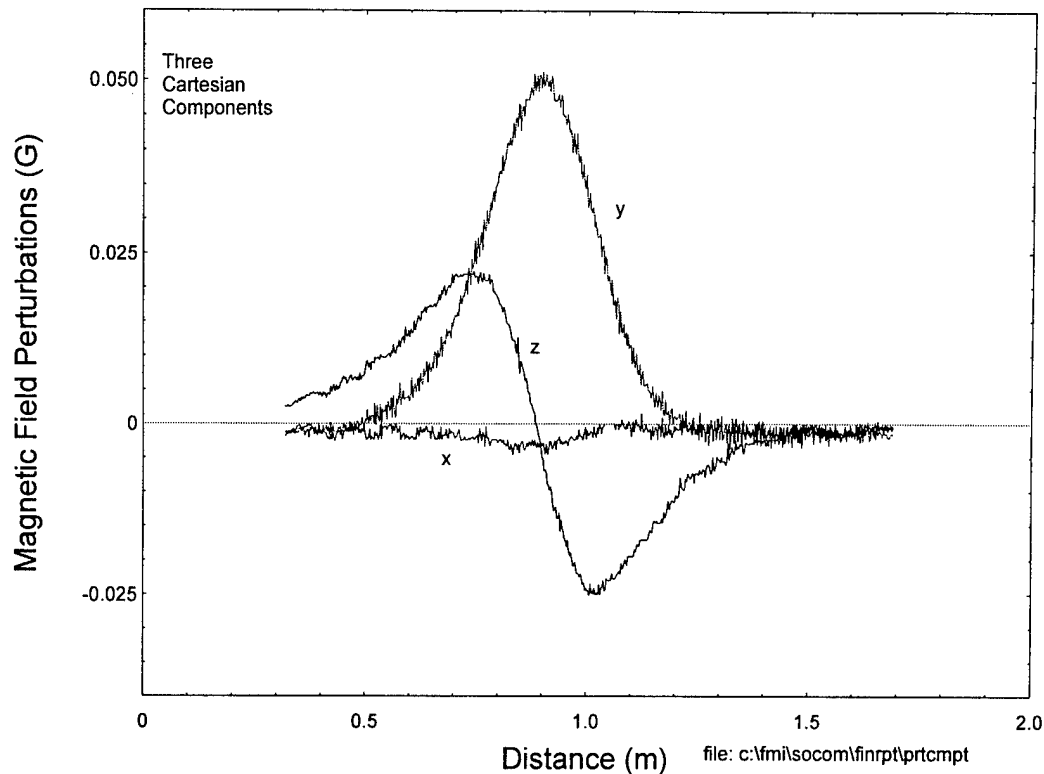
Figure 14. Measured magnetic field perturbations

4.3   Summary

The magnetic field emitted by the SDV was analyzed into component sources. There were three main contributions to the emitted magnetic field.

- Field due to the magnetic material in the electric motor.
- Field due to the operation of the motor.
- Field due to the electric currents used to drive the motor.

Magnetic field measurements were made of the SDV and a substitute laboratory motor. These measurements demonstrated that the magnetic signature of the motor was characteristic of a magnetic dipole.

The field during operation of the motor was observed to be small due to the fact that the SDV was analyzed while in dry dock and the motor could only be operated at very low current levels. When the propulsion motor is operated at the higher current levels associated with propulsion of the SDV, this magnetic field component may prove to be significant. This will have to be further studied in the Phase II program.

The field occurring during motor operation was measured. Due to the no-load aspect of the measurements, however, it is not known whether this field will increase with motor load or will remain constant. Because the loaded current may be 50A, the field may be up to 50X greater under load than at no-load. Clearly this is a crucial characteristic of the SDV which needs to be immediately determined in further work.

18

The magnetic field due to the battery pack was also small due to the small no-load current. Theoretical and numerical modeling indicate the fields will be easily detectable for currents of 10A and greater. This field is almost certainly linear with load current.

Magnetic signature conclusions based upon this data set include:

- There is significant frequency signature structure to the current trace.

- The frequency information of the measured magnetic field was dominated by the ambient 60 Hz (and harmonics) field. This is due at least in part to the low amplitude magnetic field generated by the small amplitude battery current used.

- The magnetic signature data has been correlated and combined to estimate the signature reduction needed for certain situations.

The magnetic field of an induction motor was measured in Foster-Miller's facility. The motor was used as a substitute motor for the SDV permanent magnet motor for demonstrating active magnetic shielding. The results presented here show the field to be reasonably similar to the SDV motor and also to exhibit the characteristic dipole shape of the field versus distance plots.

5. MAGNETIC ANALYSES

This section discusses the theoretical aspects of magnetic fields, including generation and cancellation, and sources of magnetic fields associated with the SDV.

5.1   General Analyses

Analyses were performed using theoretical and numerical models. The theoretical models provided estimations of the levels of field cancellation available by both deterministic and statistical approaches. In particular, in the deterministic approach, the magnetic field structure of a component (i.e. motor) was broken down into its constituent multipoles. This is a very powerful technique which determined uniquely the optimum shield coil design. In addition, a very general technique of minimization of residual field was developed for an arbitrary set of coils. Various sets of coils can be compared subsequently to determine which one offers the smallest magnetic field over the volume of interest. The numerical models simulated the overall magnetic fields emitted by the batteries.

As discussed above, measurements of the magnetic field of the SDV vehicle were made. This subsection discusses the analyses performed on the measured magnetic field data. The analyses were focused on understanding the form and function of the magnetic fields of the vehicle. Analyses were performed mainly using theoretical and numerical analyses. A third class of analyses, expert system analyses, were also performed. This last class, by its very nature, is difficult to describe and audit. Fortunately, many times an expert system analysis can be dissected and justified *ad hoc.*

Analytical approaches use theoretical methods which apply to a somewhat idealized situation, be it simplified geometry or physical properties (e.g., homogeneity, or lossless, etc.). In many cases the results exactly solve the approximate problem. The results can be generalized and perturbations to the idealized situation can be taken into account to approach some realistic situations.

Numerical approaches provide a direct means to compute a precise answer for a specific problem. The fundamental electromagnetic equations are solved by applying the appropriate boundary conditions. Numerical approaches analyze the whole problem without making simplifying assumptions.   Many times, these simulators numerically predict the fields and currents in modeled devices in less time and at less cost than actual devices could be built. Software post processors allow the engineer to "look" at data in ways which would be impossible in a real device. In addition, modifications to the modeled devices for enhanced performance are commonly much faster to achieve than hardware modifications. However, the results obtained are difficult to generalize as the designer has no direct way of determining the sensitivity of the result to specific input parameters. This means the designer must "run" several similar cases to determine the effect of a single parameter variation. Since frequently there are many independent parameters, judicious selection of the parameters to be varied must be made or else the number of computer runs becomes excessive.

The expert systems approach uses no formal calculation procedure. Instead, estimates are made of parameters of interest based upon a rules or experience database. An advantage of

this approach is that results are generally obtained quickly while disadvantages of this approach are that the results are approximate and can be difficult to trace for auditing purposes.

The theoretical models of the vehicle magnetic fields are comprised of variations and combinations of coil filament models. The purpose here is to simulate the production of a magnetic field by an applied current, permeable ferromagnetic body, or permanent magnet material.

The field due to an applied current is relatively easy to calculate. In many cases Maxwell's equations can be exactly solved and analytical equations can be written yielding an expression for the field. In other cases numerical models can be constructed and solved (described below). Even when the exact solution is available, however, it is frequently advantageous to have a machine actually compute the result.

The fields due to permeable bodies and permanent magnets can be calculated as resulting from the equivalent currents of the objects. Hence, calculation of the magnetic fields amounts to first calculating the equivalent currents and then calculating the magnetic fields from those currents.

The theoretical models are comprised of coil filaments as a fundamental building block. Equivalent currents of ferromagnetic materials are described next. These currents have obvious shielding implications since a co-located applied current which is equal but opposite to the equivalent current would exactly cancel the original magnetic field. The next subsection discusses a statistical approach to shielding—that of least squares matrix methods. Legendre polynomials represent a very powerful analytical technique similar in concept to the Fourier analysis approach. The next subsection describes how Legendre polynomials were used to shield the motor.

5.1.1 Coil Filament Models

Most analytical models are based upon an exact solution for a constant-current filament. It can be shown that the magnetic field of a circular filament of radius a at a point in space of coordinates (r,z) can be written [1]:

$$B = B_r \hat{r} + B_z \hat{z}$$

where,

$$B_r = -\frac{\mu_0 I}{2\pi} \frac{z}{r\left[(r+a)^2+z^2\right]^{1/2}} \left\{ K - \frac{r^2+a^2+z^2}{\left(r-a^2\right)+z^2} E \right\}$$

and

$$B_z = \frac{\mu_0 I}{2\pi} \frac{1}{\left[(r+a)^2+z^2\right]^{1/2}} \left\{ K - \frac{r^2-a^2+z^2}{(r-a)^2+z^2} E \right\}$$

21

K and E are the complete elliptic integrals of the first and second kind, respectively. They are defined in terms of a parameter k:

$$K = \int_0^{\pi/2} \left(1 - k^2 \sin^2 \theta\right)^{-1/2} d\theta$$

$$E = \int_0^{\pi/2} \left(1 - k^2 \sin^2 \theta\right)^{1/2} d\theta$$

$$k^2 = \frac{4ar}{(r+a)^2 + z^2}$$

In these equations r is the perpendicular distance from the coil axis and the coil is located in the z=0 plane.

Along the axis of the coil (r=0), the magnetic field is purely axial and can be written:

$$B = B_z \hat{z} = \frac{a^2 \mu_0 I}{2\left(a^2 + z^2\right)^{3/2}} \hat{z}$$

which is a relatively simple formula. The advantage of the analytical models is they permit a back-of-the-envelope calculation to estimate emitted magnetic fields. The disadvantage of these models is the lack of conformity of the idealized world and the real world (finite coil cross-section, etc.).

Computerization of the analytical models allows the formation of a bridge between the ideal and real worlds, that is, for example, the magnetic field from the finite cross-section of a coil can be calculated by dividing the cross-sectional area into many pieces and computing the filament approximation for each piece and then summing the contribution of the pieces. The elliptic integrals are approximated by a series representation as found in (2). This has been done (previously) and the resulting computer code has been proven accurate many times by direct measurement and comparison with other known-good calculations such as text book examples, far-field limits of analytical calculations (finite cross-sections matter less the further the field point is) and other computer codes—boundary and finite element.

5.1.2   Equivalent-Current Theory

The theory of equivalent currents is well established for magnetic field compensation. Magnetic field theory shows that, in principle, by the use of applied currents it is possible to exactly compensate for the induced magnetic field due to ferromagnetic bodies. The practical implementation of the applied currents and a real-time control system by which to control the currents requires a deviation from an ideal model and involves engineering tradeoffs.

In the presence of a background magnetic field, the electron spins of ferromagnetic bodies tend to become aligned in such a way as to reinforce the background field. This is a result of the torque applied by a magnetic field on a magnetic moment. Torque is also applied by a

magnetic field to a loop of current and is the basis of operation for rotating electrical machinery. This similarity suggests that the magnetic fields due to materials and due to currents can be treated on a unified basis.

The flux density within a material can be written as:

$$B = \mu H = \mu_0 (H + M)$$

where B is the flux density, μ is the material permeability, μ_0 is the permeability of vacuum, H is the magnetic field and M is the material magnetization. H is commonly created by the application of currents to a body while M describes the ferromagnetic nature of the body. Note that H and M have the same units. This equation means the magnetic flux density of electromagnets is indistinguishable from the flux density of magnetic materials.

Ampere's Law can be written and manipulated as:

$$\nabla \times H = J$$

$$H = \frac{B}{\mu_0} - M$$

$$\nabla \times \left(\frac{B}{\mu_0} - M \right) = J$$

$$\nabla \times B = \mu_0 J + \mu_0 \nabla \times M = \mu_0 J + \mu_0 J_e$$

where J_e is the equivalent volume current density of the magnetic material. By applying a current density $J = -J_e$, the net B can be made equal to the background earth field. This theory holds true for "soft" and "hard" (e.g., permanent magnets) ferromagnets, albeit with some modifications. In practice, the effect of a volume current density (A/m^2) often can be obtained with a surface current density (A/m).

There is a set of currents which will exactly reproduce the magnetic field of any ferromagnetic object. An arbitrarily shaped object will, in general, have a magnetization M induced by immersion in a magnetic field B (uniform or not). The magnetic field anomaly due to the object can be exactly duplicated by a combination of equivalent surface and volume currents when no magnetic materials are present. In addition, the magnetic anomaly of an arbitrary ferromagnetic body can be eliminated by surface and volume currents when the magnetic material is in place. This statement is true for all classes of ferromagnetic material: linear, non-linear and permanent magnet materials.

In practice, the complex applied currents are difficult to implement and some residual magnetic anomaly is, in fact, tolerable. Thus it is desirable to find a simple set of currents which reduces the magnetic anomaly to below the specified threshold. Because the specification is an anomaly less than a threshold, this set of currents need not be unique, and indeed, multiple solutions will increase the flexibility of electromagnetic design and may enhance the overall function of the shielding system.

As discussed above, an active system works with magnetostatic fields. Time variation of the fields, however, permits the introduction of quasi-static effects. In this case, an SDV with active coils can change magnetic heading. For arbitrary objects, changing the direction of the object axis with respect to the magnetic field will create a change in the magnetic field. This

change must be accounted for in the equivalent currents, and, therefore, in the compensation currents.

As an example, as a vehicle near the magnetic equator changes heading by 90 deg, the coils which were at one time facing North-South and performing the major anomaly compensation task will be facing East-West with little magnetic compensation required. Likewise, the once East-West coils will be facing North-South with greatly increased compensation currents.

Hence, the control system must know the magnitude and direction of the background field with respect to the vehicle axis in order to provide the correct compensation currents to the coils at the right time.

In conclusion, the magnetic field of an arbitrary ferromagnetic body can be exactly canceled by an appropriate set of applied currents.

Superposition of magnetic fields is fundamental to understanding how to reduce the magnetic anomaly of a body. To cancel the magnetic anomaly in the presence of a background field, the magnetic field of the body is superposed with the field due to compensation currents. If these compensation currents are chosen as described above, then the induced field of the body is exactly canceled by the compensation currents and the anomaly is eliminated.

The practical determination of the simplest set of currents which compensates best for the anomaly was discussed briefly. Recent developments in magnetic field analysis software suggest magnetic signature reduction of vehicles will become more readily accomplished in the future. It is the role of system designer to optimize the shielding integration with the vehicle and its mission.

5.1.3   Least Squares Matrix Methods

Active shielding is based upon the principle that a magnetic field can be shielded by superposition of an oppositely directed magnetic field which is created by dedicated shielding coils. The question naturally arises as to the location, size and current requirements for these coils. One approach, based more upon statistics than magnetics, is to consider the shield coil characteristics as independent parameters which may be varied and optimized without detailed knowledge of the underlying physical principles.

According to this approach, a trial location and diameter may be chosen for a shield coil and then the current selected to yield the minimum magnetic field over the desired volume. The shield current is chosen to minimize the sum of the squares of the differences between the magnetic field at a selected location due to the source and shield. For a single shield coil, the mathematical expression of the words above is:

$$\min Q = \sum_i \left(B_{source,i} - B_{shield,i} \right)^2$$

where

Q = the sum of the squares of the difference in the magnetic field, this is the quantity to be minimized

$B_{source,i}$ = the magnetic field due to the source at location i in three space (units: Tesla)

$B_{shield,i}$ = the magnetic field due to the shield coil at location i (T)

24

i   = location reference point (counter). Note that i is distributed within and on the periphery of the volume of interest.

Assuming a linear relationship between the shield current and the field produced yields the equation,

$$\min Q = \sum_i \left(B_{source,i} - K_i \cdot I_{shield} \right)^2$$

where

K_i = known constants relating shield current to shield field at each location i of interest (units: Tesla/A)

I_{shield} = the shield current to be determined (A). Note this formulation differs slightly from the usual least-squares approach in that here the constant term is forced to zero.

The constants $K_i = K(x_i, y_i, z_i)$ are determined by computing the magnetic field of the source coil geometrical configuration at locations i for a shield current of 1A. Various analytical or numerical methods are available to perform this calculation. Two methods we have used are: brute-force integration of the Biot-Savart law and, for circular coils, the numerical approximation to the elliptic integrals described above. Alternatively, a measurement of the field due to the actual coil can be performed as a calibration/verification of the calculations.

The number of locations i is arbitrary (limited only by computer memory and operator patience) and these locations can be selected in three space as desired to represent interest in particular volumes. One common technique is to select locations along a particular path representing the outline or perimeter of the volume to be shielded. The density of locations can be adjusted to represent a "weighting" or sensitivity to be applied to the shielding calculation, (e.g., increased shield performance desired below the source as opposed to the side).

The above equation is solved by setting $dQ/dI_{shield} = 0$. This yields the expression for the shield current which minimizes the sum of the squares of the differences of the magnetic fields due to the source coil and the shield coil,

$$I_{shield} = \frac{\sum_i B_{source,i} \cdot K_i}{\sum_i \left(K_i^2 \right)}$$

Similar studies have been conducted for many shielding coils, m in number. The selection of the current in multiple shielding coils is best performed by measuring the field at a number of points, n. These points are typically chosen to represent the extremes of the volume to be shielded and the number and location of points can be varied to indicate relative interest within the volume. The field produced at each measurement point by one ampere of current due to each of the shielding coils is measured to develop an influence matrix. The goal is: Given magnetic field measurements at n positions, what is the current in m shield coils which best reduces the field at each position. In matrix form we can write: [Y] = [X] • [Currents], where Currents is a vector representing the current magnitude in the m shield coils, Y is the vector of n measured points, and X is matrix relating the field due to the mth coil at the nth position. A least squares fitting routine can be used to determine the currents in each of the m

25

shielding coils. In the least squares method, the net field value is squared and summed at each point and the currents are adjusted to minimize the total sum. Figure 15 summarizes this formulation.

If the field 'shape' or harmonic content is invariant as the vehicle operates, then the ratio of the currents in the shield coils will not vary and can be pre-determined. Note, however, that eddy currents and other nonlinear effects could require the adjustment of the relative currents in the set of shield coils. The above formulation is a simple and efficient method for rapidly determining the desired current in m coils fitting to n data points where $n >= m$.

This approach is most useful if it is desired to have a shield which can be re-configured as a result of unpredictably changing sources. There are two major tradeoffs with this approach: the shielding is likely non-optimum for any single configuration of sources and the maximum magnetic anomaly (i.e., maximum stray magnetic field) is not known.

Because of the success in analyzing the physics of the field structure mathematically as described in the next subsection, this statistical technique was not used in practice. Notwithstanding this decision, this is a powerful technique which may be employed in situations where the geometries are complicated and the physics and mathematics are not so accommodating.

Currents $\left(X^T \cdot X\right)^{-1} \cdot \left(X^T \cdot Y\right)$

Y = Unshielded Field =

$$
\begin{bmatrix}
Yz1 \\
Yz2 \\
.... \\
.... \\
Yzn \\
Yr1 \\
Yr2 \\
.... \\
Ym
\end{bmatrix}
$$

X = Influence Matrix =

$$
\begin{bmatrix}
Bz11 & Bz12 & .... & ...... & Bz1m \\
Bz21 & Bz22 & .... & ...... & .... \\
Bz31 & .... & .... & .... & ...... \\
..... & .... & .... & ...... & ..... \\
Bzn1 & Bzn2 & .... & ...... & Bznm \\
Br11 & Br12 & .... & ...... & Br1m \\
Br21 & Br22 & .... & ...... & .... \\
Br31 & .... & .... & .... & ...... \\
..... & .... & .... & ...... & ..... \\
Bm1 & Bm2 & .... & ...... & Bmm
\end{bmatrix}
$$

Currents =

$$
\begin{bmatrix}
I1 \\
I2 \\
.... \\
.... \\
.... \\
.... \\
.... \\
Im
\end{bmatrix}
$$

(arb. location)

Bz12 = z directed field at point 1 due to one ampere in coil 2

Yr1 = r directed field at point 1 before shielding

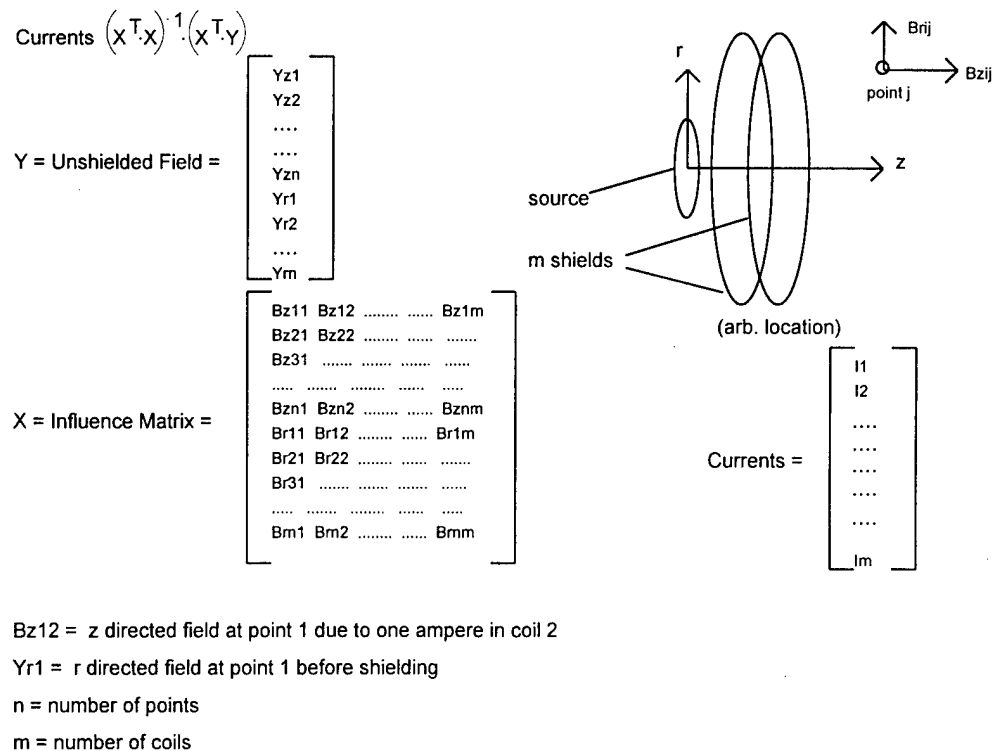n = number of points

m = number of coils

Figure 15. Geometry and math of multiple shielding coils

26

5.1.4 Legendre Polynomials

The basis for shield coil design for various components (such as the motor) was the breakdown of the magnetic field of the source into contributing multipole moments. The shield coil is designed to create a field equal and opposite to the source field—in this case the permanent magnet field. In principle, it is always possible to exactly cancel a given magnetic field by applying currents equal and opposite to the equivalent currents of the source. However, as a practical matter, the geometry severely restricts the coil placement options. Fortunately, it turns out that the desired shield coil location is actually available with the given geometry of the motor.

Conceptually, it is of interest to identify the contribution of multipoles to the magnetic field of the motor, i.e., to what extent is the magnetic field dipole-like, quadrupole-like, octupole-like, and so on. The analysis and measurements discussed in this section define and quantify the motor multipole distribution.

A dipole magnetic field is simply that due to a loop of current at a distance large compared to the loop radius. A quadrupole field may be thought of as two equal and opposite dipoles (two loops of opposite current) separated by a distance. In fact, a multipole of order n can be assembled from multipoles of order (n-1) in this manner (inverted and slightly separated).

For this development, the following assumptions have been made: the media is homogenous, isotropic and linear. Since we shall be applying the results to air these assumptions are very good indeed. It can be shown that the magnetic field satisfies the following equation (3):

$$\nabla^2 \mathbf{B} - \mu\varepsilon \frac{\partial^2 \mathbf{B}}{\partial t^2} = \mu \nabla \times \mathbf{J}$$

where

μ = media permeability
ε = media permittivity
J = source current

For the further assumptions of no sources in the media (J=0) and quasistatic analysis ($\lambda \gg$ L, or $\partial^2/\partial t^2 \to 0$) we have:

$$\nabla^2 \mathbf{B} = 0$$

Note this equation involves the vector Laplacian. In rectangular coordinates each component is separate,

$$\nabla^2 B_i = 0, i = x,y,z \text{ (rectangular coords)}$$

The expansion of vector Laplacian components for curvilinear coordinates is more complicated than the rectangular coordinates with the exception of the axial component in cylindrical coordinates.

$$\nabla^2 B_z = 0 \text{ (cylindrical coords)}$$

The axial magnetic field satisfies Laplace's equations in regions outside of current or permanent magnet sources. There is a family of mathematical polynomials, infinite in extent,

referred to as the Legendre polynomials, $P_n(x)$, which satisfy Laplace's equations in the case of azimuthal symmetry.   It can be shown that these polynomials form a complete orthonormal set of functions. This means that *any* function ("complete") satisfying Laplace's equation can be expanded in a *unique* ("orthonormal") series of Legendre polynomials. Of particular interest is that fact that the axial magnetic field of the motor with magnetic material surrounding it can be represented in a unique Legendre series. [For non-axisymmetric situations there is an extended set (a superset) of polynomials, the associated Legendre polynomials, $P_n^m(x)$ which possess analogous properties.]

The Legendre polynomials are a function of a parameter (x) which varies from +1 to -1. Convenient identification allows an angle variable to be used such that: $x = \cos(\theta)$, where θ varies from $\theta = 0$ to $\theta = \pi$. While the index, n, for the Legendre polynomials ranges from 0 to infinity, the analysis was done with the index ranging from 2 to 6. The first six Legendre polynomials are given in Table 2 (4).

Alternatively, it can be shown that based upon the physics of the problem, the magnetic field can be expressed as a sum of the contributions from a uniform field, a monopole field, dipole field, quadrupole field, octupole field, etc. as

$$B(r) = B^{(0)}(r) + B^{(1)}(r) + B^{(2)}(r) + B^{(3)}(r) + B^{(4)}(r) + \ldots$$

respectively. This is shown schematically in Figure 16. [Note that the monopole magnetic field can be shown theoretically to be equal to zero. The same formalism applies to electric or

Table 2.   Legendre polynomials

Index, n	Legendre Polynomials, $P_n(\cos(\theta))$
0	1
1	$\cos(\theta)$
2	$1/2 \, (3 \cos^2(\theta) - 1)$
3	$1/2 \, (5 \cos^3(\theta) - 3 \cos(\theta))$
4	$1/8 \, (35 \cos^4(\theta) - 30 \cos^2(\theta) + 3)$
5	$1/8 \, (63 \cos^5(\theta) - 70 \cos^3(\theta) + 15 \cos(\theta))$
6	$1/16 \, (231 \cos^6(\theta) - 315 \cos^4(\theta) + 105 \cos^2(\theta) - 5)$
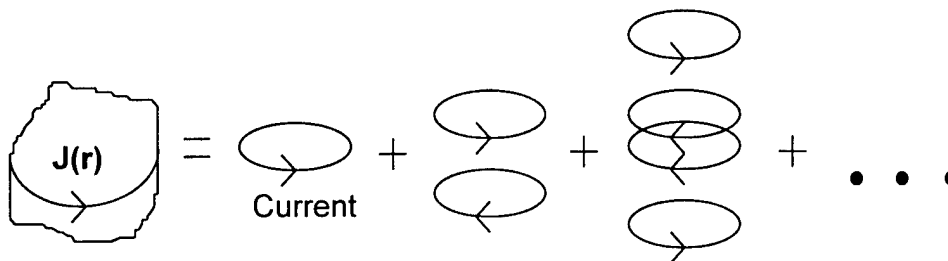
Arb. Source $=$ Dipole$+$ Quadrupole$+$ Octupole$+$ (higher order moments)

Figure 16. Schematic expansion of arbitrary source into multipole components

28

acoustic fields and in this case the monopole field need not be zero.] It is relatively easy to demonstrate that a dipole axial field corresponds to $P_2(\cos\theta)$, a quadrupole to $P_3(\cos\theta)$, and so on, but it is beyond the scope here.

Figure 17 shows polar plots of the dipole, quadrupole and octupole moments. Note that, as usual, the zero angle ($\theta = 0$) corresponds to the horizontal axis. The plots are for $0 \leq \theta \leq \pi$.

At distances far from the location of the magnetic anomaly compared to the size of the ferromagnetic body producing the perturbation (in this case, 9 in.), the magnetic field can be shown to be dipolar in nature. Thus, the appropriate current source to cancel this magnetic field would be that of a simple current loop. This facilitates the cancellation of the magnetic anomaly field using simple current loops.

In summary, the axial magnetic field must satisfy Laplace's equation and therefore can be written as:

$$B_z(r) = \sum_{n=0}^{\infty} A_n r^{-(n+1)} P_n\big(\cos(\theta)\big)$$

where we seek to determine the coefficients A_n. The relative magnitude of the coefficients will determine the relative importance of the various n-poles.

In summary of technique, mathematically we can extract the dipole term from the Legendre expansion much like the fundamental frequency can be extracted from a Fourier series expansion. Both techniques highlight the effect of the higher order effects, in one case magnetic field multipole and in the other case harmonics of the fundamental. Any real source, of course, is composed of contributions of various multipole components.
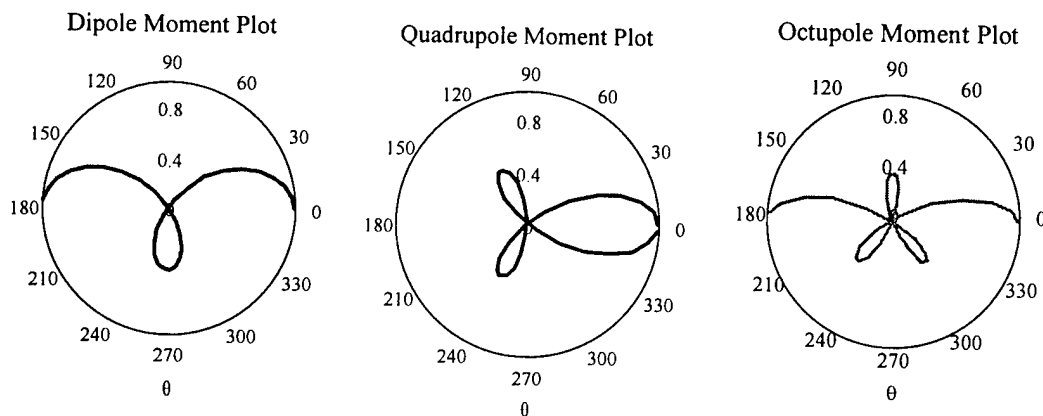

Figure 17. Polar plots of multipole moments

5.1.5 Conductor Transmission Lines

Magnetic fields are created whenever currents flow in conductor wires. The magnitude of the magnetic field observed depends upon the current level within the wire, the geometry (or shape) of the wire and the distance from the wire of the observer. Figure 18 shows typical variations in magnetic field with increasing distance for transmission lines of different geometries. Constant total current is assumed. Note that the rate of decay in amplitude depends remarkably upon the conductor geometrical distribution.

A simplified calculation of the magnetic field from a battery cable and its return path will illustrate some of the issues involved. Shown in Figure 19 are two cables with a supply and return current I. For simplicity, the calculation assumes the battery cables are infinitely long. We shall see that the range at which detection is possible is great, indeed. Since the SDV itself is of a certain length, the large detection range invalidates the infinitely long assumption and suggests a more refined calculation is in order. The center-to-center spacing of the cables is d and the cable length is l. The vertical magnetic field is calculated at a vertical distance z below the cables. The magnetic field for infinitely long cables is given by the expression:

$$B_{net} = \frac{2\mu_0 I}{2\pi r} \cos(\theta)$$

$$\cos(\theta) = \frac{d/2}{r}$$

This model will be useful when calculating the fields emitted from the cables of the battery pack of the SDV.
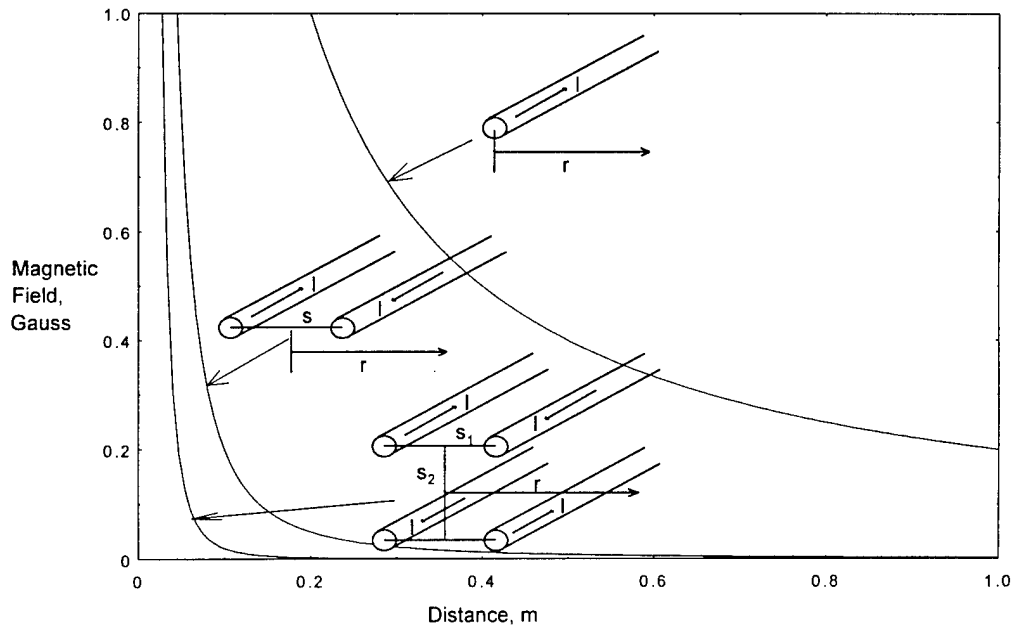

Figure 18.   Transmission line magnetic field versus distance

5.2   Specific Analyses for the SDV

In this program, three sources of magnetic field signature have been identified emitting from the SDV:

- Magnetic field anomaly due to ferromagnetic mass (primarily due to the motor).

- Magnetic fields of the battery currents.

- Magnetic fields of the running motor.

This section describes the contribution from each of these three sources, discusses their relative contribution to the far field magnetic field, and calculates the range at which these contributions may be detected assuming a specified level of magnetic field detection.

Figure 19.   Geometry for magnetic field calculation of parallel arrangement of long battery cables

Assuming a low magnetic noise environment and a measurement threshold of 1 nT (one nano-Tesla), estimates of the radii of observability have been made for each of the three sources in isolation. The range calculations are given in Table 3 below. Figure 20 illustrates the radii of observability for these sources (roughly to relative scale).

Based upon the level of magnetic field measured or calculated, the unshielded SDV will be readily observable at distances from the vehicle from 14m (= 46 ft) to 18.5m (= 61 ft),

Table 3.   Summary of SDV sources, uncorrected fields and unshielded observability ranges*

Battery Cables	Ferromagnetic Motor Mass	Motor Field
$B = \dfrac{\mu_0 I d}{2\pi r^2}$ "Long" $B = \dfrac{\mu_0 I d \cdot l}{2\pi r^3}$ "Short"	$B = \dfrac{\mu_0 m}{2\pi r^3}$	$B = \dfrac{B_0 r_0^3}{r^3}$
$d \sim 3$ in., $l \sim 5$m, $I \sim 50$A	$m \sim 12$ A-m^2	(a) $B_0 \sim 2$ mG, (b) $B_0 \sim 50 \times 2$ mG $r_0 = 0.775$m
$r \sim 14.7$m $= 48$ ft	$r \sim 14$m $= 46$ ft	(a) $r \sim 4.5$m $= 15$ ft (b) $r \sim 16.7$m $= 55$ ft

*Note: these formulas calculate peak dipole fields

31

Figure 20. Schematic of field source and radii of observability

depending upon operating conditions. Stated another way, if the SDV travels without power along the water's surface, a magnetically-influenced mine on the seabed can detect the presence of an unshielded SDV for all water depths less than 46 ft.

5.2.1   Fields Due to Motor Ducting

When a ferromagnetic body is placed in a magnetic field (such as the earth's background magnetic field), the highly permeable material causes a distortion in the magnetic field lines. This distortion to the field is termed the magnetic anomaly. Figure 21 shows the resulting magnetic field lines of a ferromagnetic body placed in a magnetic field that had been initially uniform.

Figure 21 shows how the magnetic field lines are "drawn" into the ferromagnetic body and distorted away from the straight line paths that they would otherwise follow in the uniform field condition. This phenomenon is referred to as ducting in analogy with the fluid streamlines within an air- or water-duct. For the magnetic case, it is energetically favorable for the field lines to pass through the ferromagnetic object. This causes the lines to converge—and then diverge—relative to the object. The distortion of the magnetic field lines results in a perturbation of the magnetic field vector direction and magnitude.

These magnetic field perturbations can be detected using magnetic field sensors, thus betraying the presence of the ferromagnetic body as well as its location and size.

For a simple steel target (i.e. a ferromagnetic motor used to power an SDV), the perturbation to the ambient magnetic field, B_0, would possess the dominant characteristics of a magnetic dipole. Assuming that the magnetic material can be approximated as spherical, the magnetic field perturbation to the ambient field is described by the equation (in cylindrical coordinates):
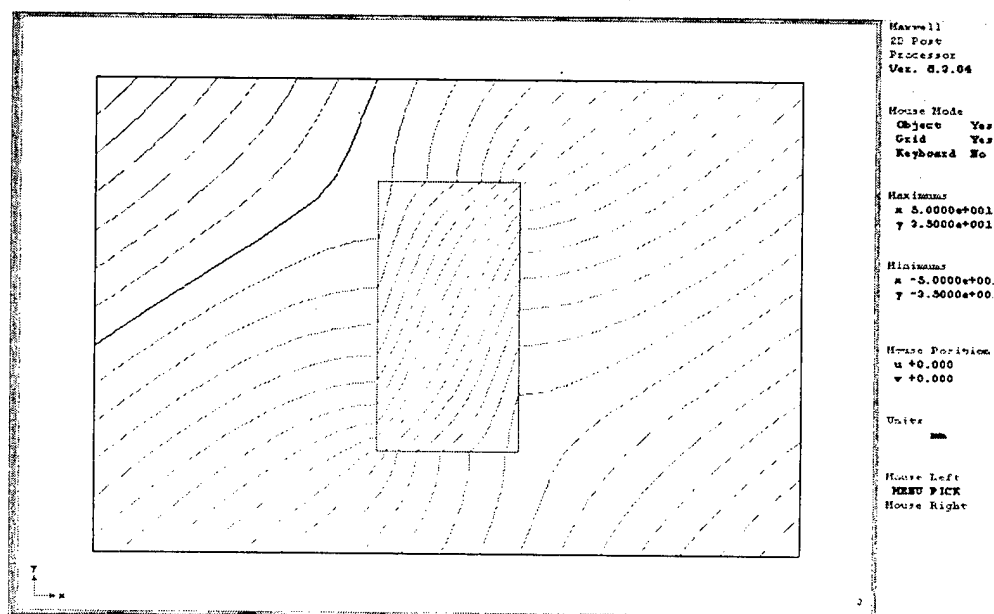

Figure 21.   Magnetic field lines in presence of ferromagnetic body

33

$$\Delta B = B_0 \cdot \left(\frac{R}{r}\right)^3 \left(2 \cdot \hat{r} \cdot \cos(\theta) + \hat{\theta} \cdot \sin(\theta)\right)$$

Where:

ΔB = the perturbation to the ambient magnetic field
B_0 = the ambient magnetic field level
R = the effective average radius of the magnetic material
r = the distance to the field measurement
θ = the angle between the ambient magnetic field direction and the direction to the field measurement location

If the magnetometer array passed directly above the "Pole" of the target's magnetic signature with its axis aligned along the ambient field, the magnetic field component measured along each of the three axes would show variations due to the presence of the target. These characteristics are well documented and predictable. These patterns are shown in Figure 22 which presents the three vector components of the magnetic field as a function of distance traveled by the magnetometer array. The three curves presented in Figure 22 show the characteristic signature of a magnetic dipole target.

5.2.2 Fields Due to Battery Currents

Models were used to represent the physical battery pack in magnetic analysis software. This was done as an alternative to shielding the actual battery pack for reasons of economics and spare battery pack availability. In this case, the magnetic field generated by a single battery tray was modeled numerically. The major purpose of this effort was to determine the
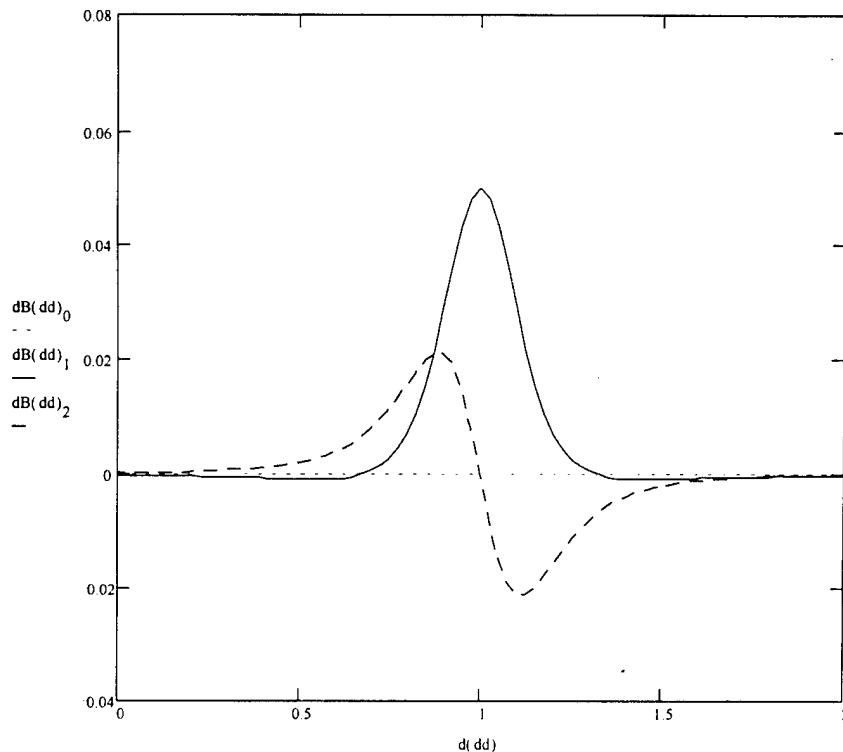

Figure 22. Predicted magnetic field perturbations

34

magnetic characteristics associated with the given geometry (i.e., the conductor paths) of the actual tray and to devise alternate geometries which reduced the magnetic field. The changes to the conductor paths were traded-off against the achieved reduction in magnetic field. As we shall see, this tradeoff of residual field versus conductor placement becomes an important aspect of the system.

In this section, the re-routing of the SDV battery cables will be analyzed. Three-dimensional magnetic analysis software was utilized to predict the magnetic signature reduction that can be achieved though a redesign of the electric current routing in the SDV battery trays. Two different battery tray configurations were analyzed corresponding to an "original" configuration and the "present" configuration.

Returning to the calculation of the stray field emitted by the battery cables of the battery pack. When the distance d = 3 in. = 0.0635m, and z = 30.5 in. = 0.775m, then $B_{net}/I = 21$ nT/A. For the measured no-load Run current of 0.9A, the estimated field is 19 nT. This value was just below the standard minimum sensitivity of our data acquisition system of 20 nT (±5V measurement with a 12 bit D/A and 0.1 G/V scaling). Thus, the magnetic field from the no-load current in the battery cable is about equal to the threshold for measurements. Increasing the current to better represent actual motor load conditions would make the field easily measurable. Typical loaded-motor currents are 50 to 100A, thus increasing the magnetic field signal by a factor of 55 to 110.

From the above equations, it can be seen that $B \sim 1/r^2$ for idealized long and straight transmission lines. It is possible to predict the distance within which the magnetic field will be greater than a critical value. If we assume the motor current is 50A and the critical field is $B_c = 1$ nT, then within a radius $r_c = 25m = 82$ ft of the infinitely long cables the magnetic field is greater than the critical field. Because the battery cables actually form a loop of approximately 5m in length, a dipole approximation, $B \sim 1/r^3$, to the field is needed, as shown in Table 3. In this case, if the detection threshold is 1 nT, the SDV is detectable due to battery currents of 50A within 14.7m (48 ft).

For arbitrary electric current paths, the dipole contribution to the magnetic field can be shown to be proportional to the area enclosed by the current path. Since the magnetic field observed far away from the object is chiefly dependent upon the amplitude of the dipole moment, it is important to minimize the area enclosed by the current loop. This is the basis of intelligent current routing for magnetic signature reduction.

5.2.3   Motor Running Fields

The magnetic field of the no-load operating motor was measured and compared to the motor Off condition. A field of 2 mG was measured at a distance of 0.775m from the motor center. It is presently not known how this field varies with load current. (The no-load current was 0.9A.)

To bound the likely possibilities, two cases were considered: constant field (load current-independent), and, field linearly dependent upon load current. When the motor is loaded at 50A, the former assumption results, of course, in a field of 2 mG at 0.775m while the latter assumption results in 100 mG at 0.775m. Assuming a dipole-like field, the detection ranges can be calculated for each case. Table 3 gives the results: 4.5m detection range for the former case and 16.7m for the latter case. The ratio between these distances corresponds to the cube-root of the ratio of currents (50X, 3.68=$50^{1/3}$).

5.2.4   Other Sources

The above sources were measured under no-load conditions. It is possible that other sources exist but were too small to be separately identified. Two such likely sources of field are briefly discussed here. The first is other ferromagnetic objects contained within the SDV. The second possible additional source is the motor controller. Any magnetic field associated with the controller this device is expected to be of high frequency (several kiloHertz). This fact makes shielding significantly easier both for the inherent shielding performed by ordinary metal boxes and for dedicated shielding efforts should the inherent shield by found inadequate.

The additional ferromagnetic objects may be associated with the SDV itself or may be mission-dependent. In particular, during informal discussions the existence of a transformer was discussed. Further investigation is certainly called for to determine the size and location of any additional ferromagnetic objects.

The signature of the motor controller has not been measured and is only mentioned as a potential source. However, if the controller has a detectable signature it is likely to be a unique "fingerprint" which may compromise the stealth mission. Again, further investigation, including high frequency (5 to 20 kHz) measurements made under motor load, is required to determine whether any controller-related signature exists.

5.3   Summary

There are three dominant sources of magnetic field signature which have been identified emitting from the SDV under no-load:

- Magnetic fields of the battery currents.
- Magnetic field anomaly due to ferromagnetic mass.
- Magnetic fields of the running motor.

The magnetic fields of the battery currents are determined from the conductor geometry and current magnitude. Any spatial separation between the current supply and return path can create a significant magnetic field which will decrease very slowly with increasing distances. Just as with the battery pack, proper transmission line routing can significantly reduce this type of emitted magnetic field.

The presence of a ferromagnetic body will distort the ambient magnetic field due to the ducting of magnetic field lines. These field perturbations are predominantly that of a magnetic dipole. Reduction of this magnetic field necessitates active magnetic cancellation.

It is possible additional sources will be uncovered when the motor is operated under significant-load conditions. Other sources of undesired magnetic field perturbations include the SDV motor controller.

The magnetic field emitted by operation of the electric motor was small due to the extremely low currents used during measurements. The field under motor load will have to be measured and analyzed further in the Phase II program.

A preliminary analysis of the magnetic field data has been performed and the results indicate the largest magnetic field is due the mass of ferromagnetic material represented by the motor. The measured magnetic field had little to do with the *type* of motor, but was mainly dependent upon the length and diameter of the ferromagnetic material.

6. MAGNETIC SHIELDING DESIGN AND SYSTEM INTEGRATION

Foster-Miller's design philosophy for difficult problems such as magnetic shielding for the SDV is twofold: 1) innovative applications of today's' technology is the key to success, and 2) strongly linked industrial R&D and manufacturing is essential. The application of this philosophy resulted in different approaches for different shielding applications within the overall vehicle. The main emphasis was on discovering what performance was achievable at a reasonable co:.t. Exotic solutions were considered only to the extent that they indicated fundamental shielding limits since they have a significant negative cost impact.

Magnetic shielding of two types was demonstrated: passive conductor cable re-wiring and active magnetic field cancellation. The conductor cable re-wiring was performed numerically and the active shielding was demonstrated on a substitute motor in our laboratory.

6.1 Passive Conductor Rewiring

The stray magnetic field dependence on the enclosed loop area has been demonstrated previously. The battery conductor configuration can reduce the area enclosed by the current loop. The principle introduced there was to get the supply and return cables as close to each other as possible.

In this section we discuss the shielding results of the Original and Present battery pack wiring configurations. In summary, the results show a magnetic field signature reduction of between 12 and 15 dB can readily be obtained depending upon the starting configuration. The results also show the fairly sensitive nature of the residual field to the precise positioning of the conductors.

6.1.1 Original and Original-Shielded Battery Configurations

When the original battery tray electric current configuration was analyzed, it was found that there was a large spatial separation of the electric conductors from the batteries and its return path. As discussed earlier, this separation leads to a significant area enclosed by the electric current and thus leads to a large magnetic dipole moment, which translates into a large magnetic field signature. Since the magnetic field measured far from the SDV is chiefly dependent upon the amplitude of the dipole moment, it is desirable to minimize it by minimizing the enclosed area, i.e., minimizing the separation between these conductors. This analysis lead to the redesign of the original battery tray configuration.

A schematic of the Original Battery Pack configuration was previously shown in Figure 2. Figure 23 shows the geometry of the numerical model was which used to predict the stray emitted field of this battery pack configuration. Note: the conduction path has been closed.

Figure 24 shows some results of the predicted stray magnetic field from this model. A contour plot is shown of the vertical magnetic field at a distance of 1m from the battery pack. Indicated by gray-levels are areas of constant vertical field. This field component is shown

Figure 23.   Geometry of numerical model for original configuration

"Forward"
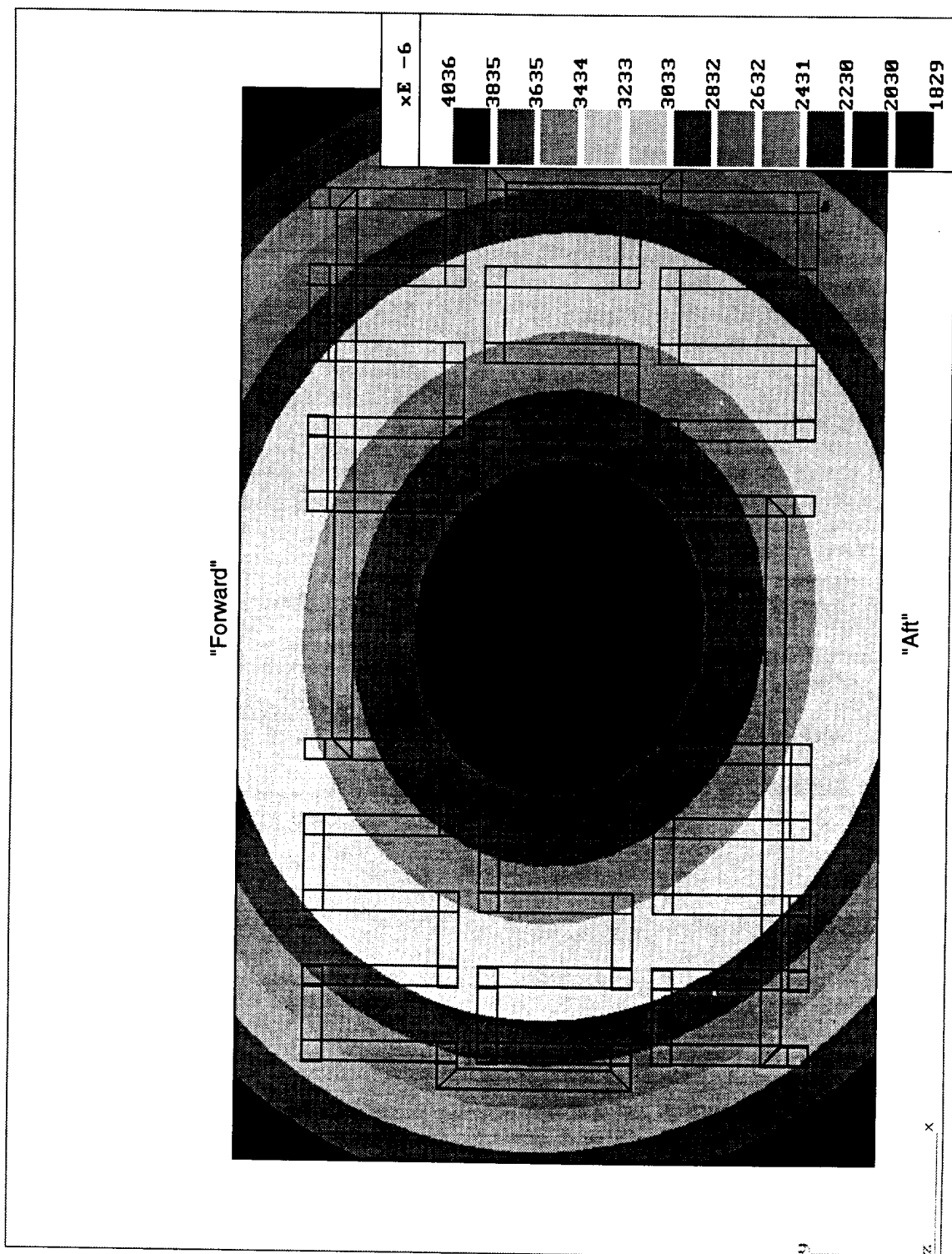
"Aft"
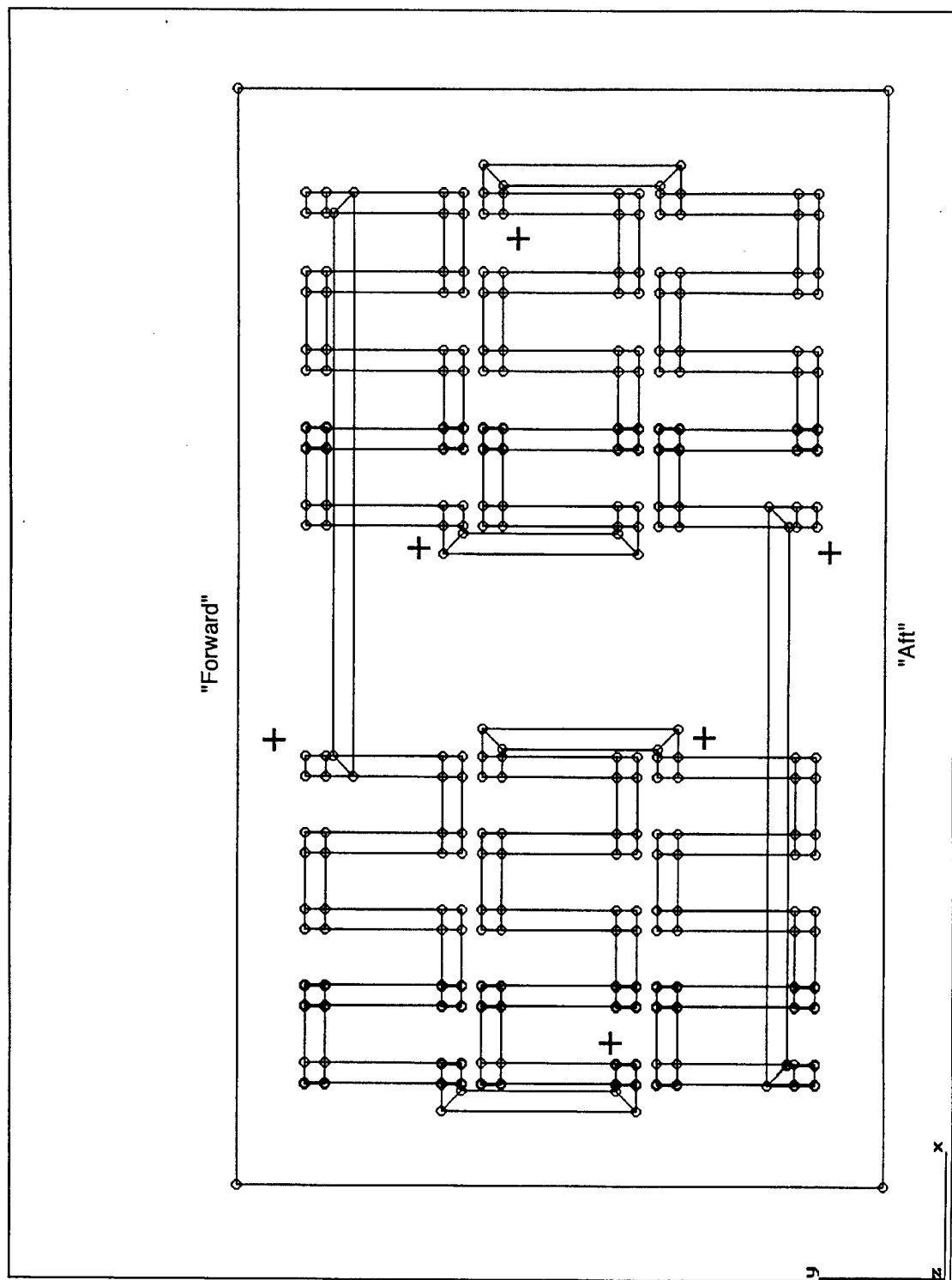
355-SOC-96025-2

Figure 24. *Vertical field contour plot for original configuration at 1m*

"Forward"

"Aft"

xE -6

4036
3835
3635
3434
3233
3033
2832
2632
2431
2230
2030
1829

since it is of the greatest concern for mine fuzing. The peak magnetic field magnitude,

$$|B| = \sqrt{B_x^2 + B_y^2 + B_z^2}$$

in this plane was 4 mG (milliGauss) = 400 nT. The battery current modeled was 100A. The units on the figure are microGauss.

The redesign of the conductor paths occurred with minimal perturbation to the batteries and connection themselves. This redesign is presented schematically in Figure 25 and the numerical model is shown in Figure 26.

Figure 27 shows some results of the predicted stray magnetic field from this model. A contour plot is shown of the vertical magnetic field at a distance of 1m from the battery pack. Indicated by gray-levels are areas of constant vertical field. This field component is shown since it is of the greatest concern for mine fuzing. The peak magnetic field magnitude, $|B|$, in this plane was 0.7 mG = 70 nT for the same battery current. The units on the figure are 0.1 microGauss.

The shielding therefore reduce the field of the original configuration from 4 mG to 0.7 mG for a reduction factor of 5.7:1 and a figure of merit of -15 dB

$$\left(= 20 \ \log\left(\frac{B_2}{B_1}\right) \right).$$

Figure 25. Schematic redesign of original battery tray configuration

This redesign also results in minimal perturbation to the cabling of the battery and its associated connections.

6.1.2 Present and Present-Shielded Battery Configurations

The present battery configuration has a much smaller separation between the supply conductors and the return path. This routing, however, could still be significantly improved in order to minimize the emitted magnetic field.

The conductors within the battery pack are presently not secured within the battery. Hence the conductors could vary in position during a mission thereby changing the stray field. Hence, on an inbound leg of a mission the stray field could be within acceptable limits but on the outbound leg the stray field could have changed significantly such that the field is above the allowable threshold.
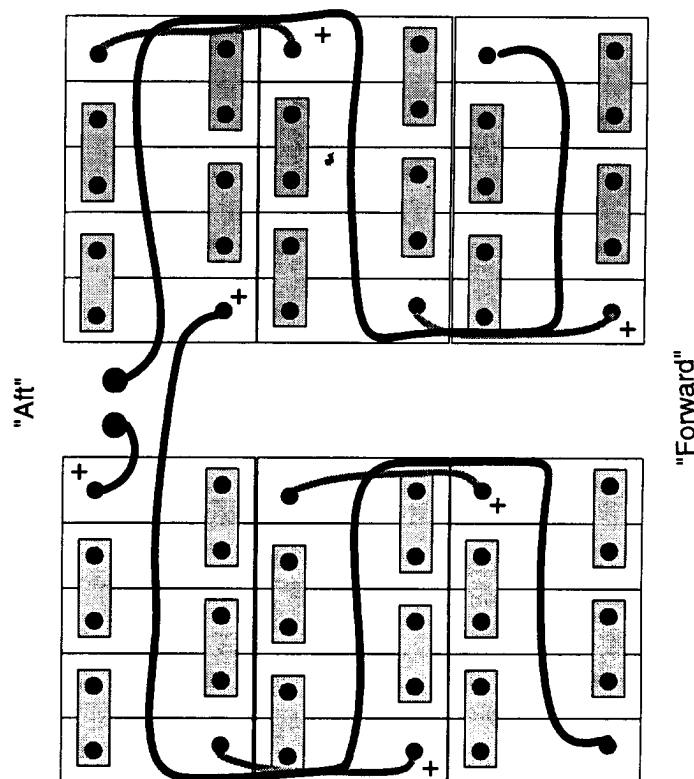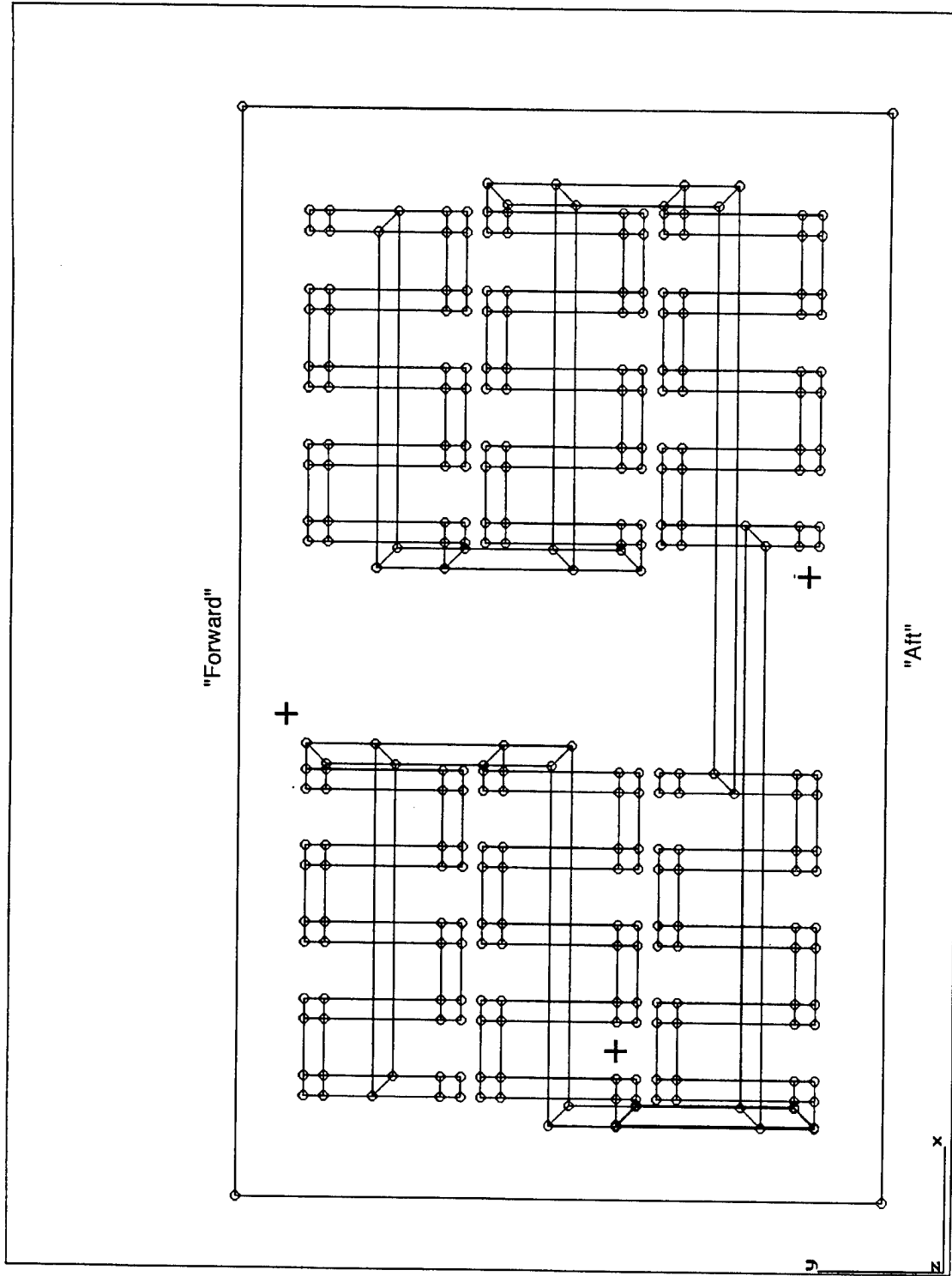
"Forward"

"Aft"

355-SOC96025-1

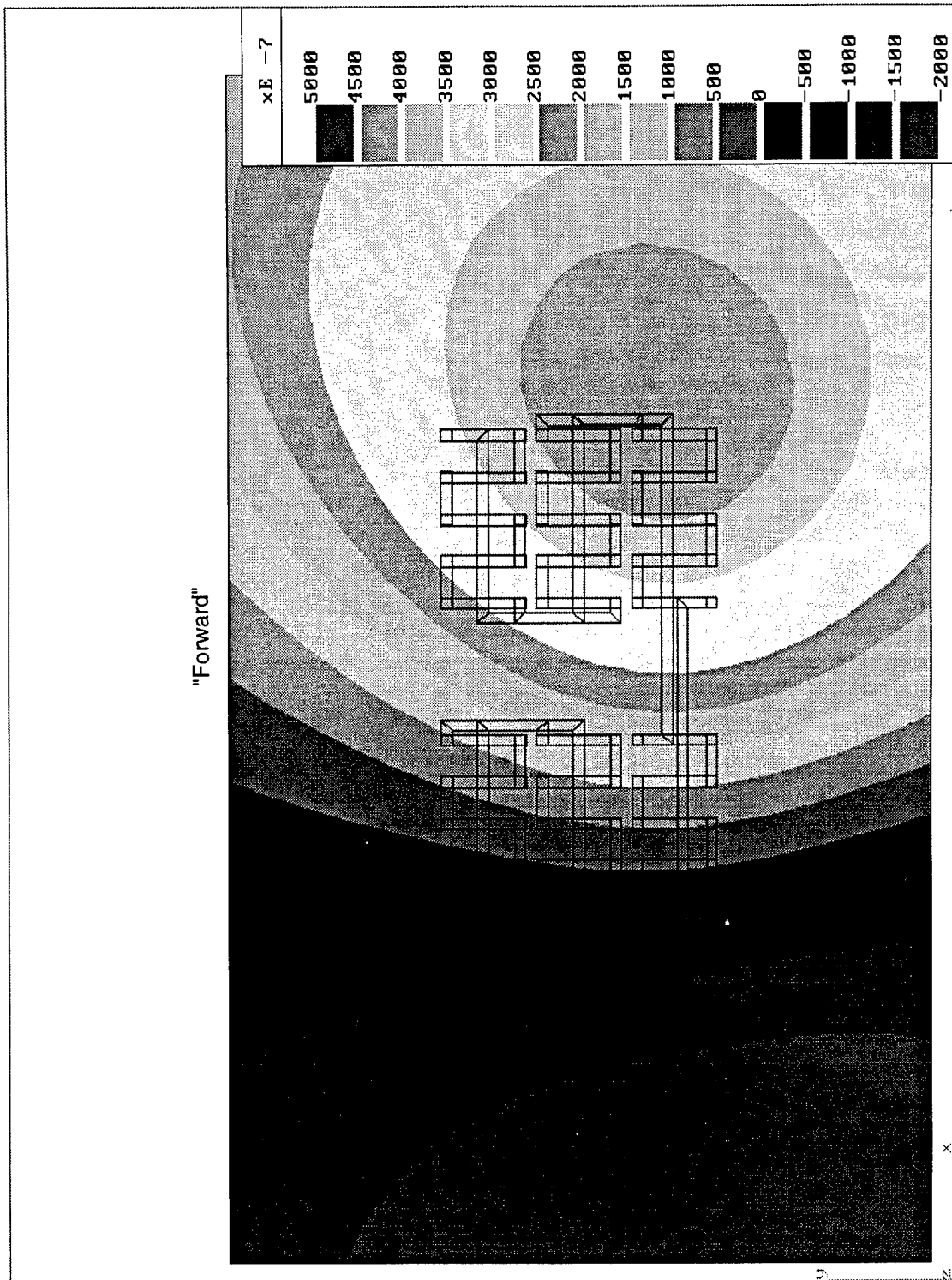*Figure 26. Geometry of numerical model for shielded original configuration*

41

Figure 27. *Vertical field contour plot for shielded-original configuration at 1m*

A schematic of the Present Battery Pack configuration was previously shown in Figure 4. Figure 28 shows the geometry of the numerical model was which used to predict the stray emitted field of this battery pack configuration.

Figure 29 shows some results of the predicted stray magnetic field from this model. A contour plot is shown of the vertical magnetic field at a distance of 1m from the battery pack. Indicated by gray-levels are areas of constant vertical field. This field component is shown since it is of the greatest concern for mine fuzing. The peak magnetic field magnitude, $|B|$, in this plane was 2.7 mG (milliGauss) = 270 nT. The battery current modeled was the same as above, 100A.

A shielded battery pack configuration has already been exhibited which has significantly lower magnetic field emissions than the Present configuration (0.7 mG shielded versus 2.7 mG Present configuration). Therefore, although it is possible to show a configuration with still-lower stray field, it seemed more useful to indicate the *sensitivity* of the stray field to the precise location of the conductors.

Figure 30 shows the numerical model for a slightly modified Present configuration battery pack. The slight modification is the highlighted conductors each have been moved a distance of approximately 3/8 in. compared to the baseline Present configuration. The conductors are not well-secured and this is less distance than the conductors might move under inertial forces (i.e., sudden athwartship or longitudinal acceleration). Figure 31 shows the predicted stray field of the slightly modified configuration. For the same current, the peak magnetic field magnitude, $|B|$, in this plane was 2.3 mG (milliGauss) = 230 nT.

Comparisons of Figure 29 and Figure 31 suggest quite different stray magnetic fields caused by a relatively small change in conductor configuration. The important point here is that whatever field might be numerically predicted, the real task is to reduce the stray field of the SDV *reliably* during a mission. In order to withstand the rigors of missions, the conductors must be well-secured in order to gain the predicted benefit in magnetic field suppression.

6.1.3   Summary

A 15 dB reduction (5.7:1) in magnetic field was numerically predicted through a re-routing of the battery cables associated with the Original configuration. A 12 dB reduction (4:1) in magnetic field was predicted through a rerouting of the battery cables associated with the present design. The precise location of the conductors is extremely important and the conductors must be well-secured to gain the calculated magnetic signature reduction.

6.2   Active Cancellation Circuit Description

The active cancellation system used in the experimental demonstration of the magnetic signature reduction system consisted of a simple negative-feedback loop. The magnetic field was sensed in the immediate vicinity of the electric motor and compared to the ambient magnetic field measured far from the motor. The difference between these two measurements was amplified by a high gain amplifier and used to drive current through an appropriate set of cancellation coils. The coils used to enact the active cancellation consisted of three coils of wire (AWG 24) wound around the motor around the center of all three of its principal axes. Each coil in this arrangement was used to independently control the dipole moment of the magnetic field associated with a particular Cartesian component.

Figure 32 shows a conceptual schematic of the active control system. The basic idea is the magnetic field emitted from a source (shown as a solenoid for simplicity) is measured by a sensor. The output of the sensor is amplified and conditioned and drives a power supply which
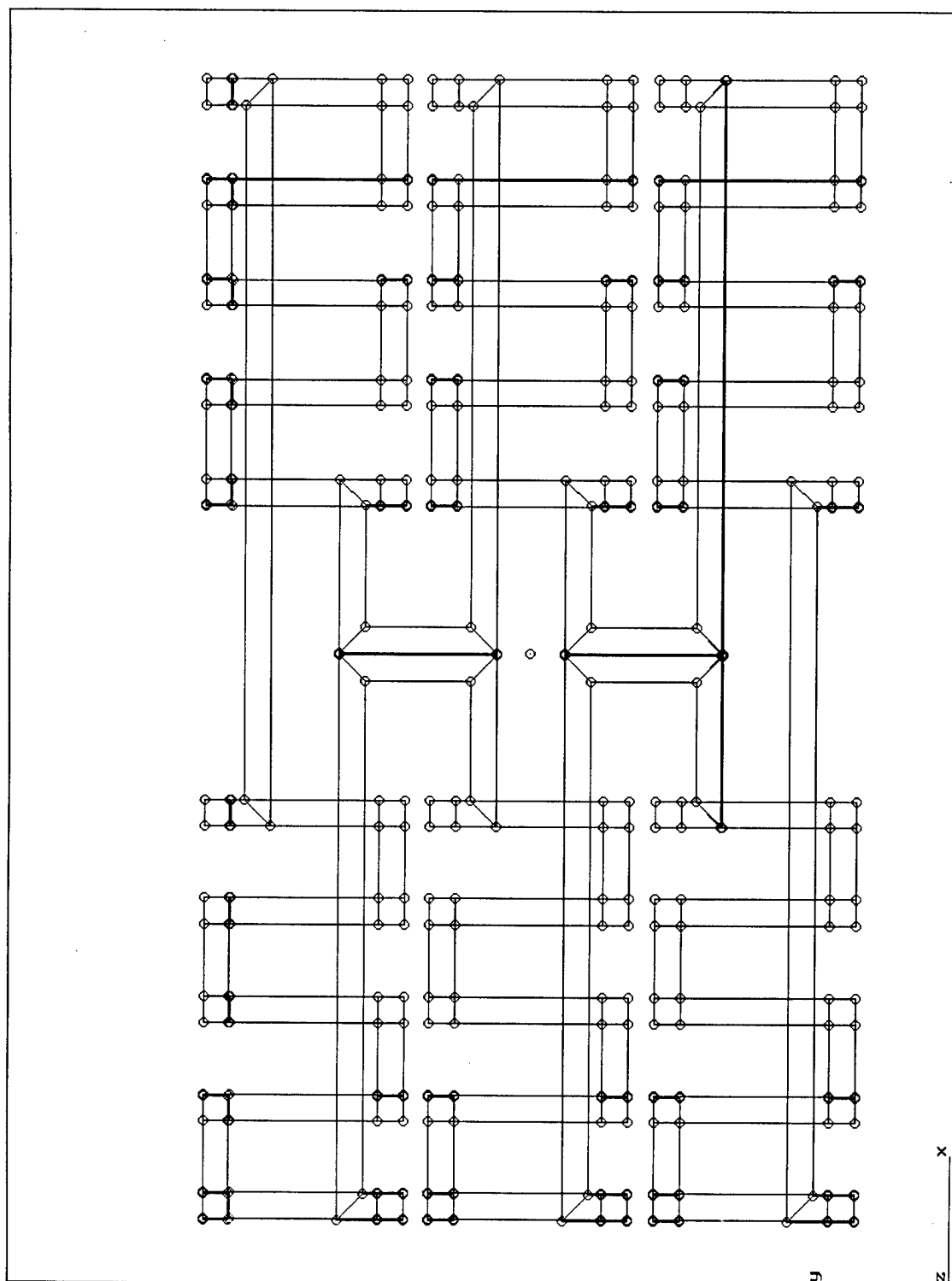
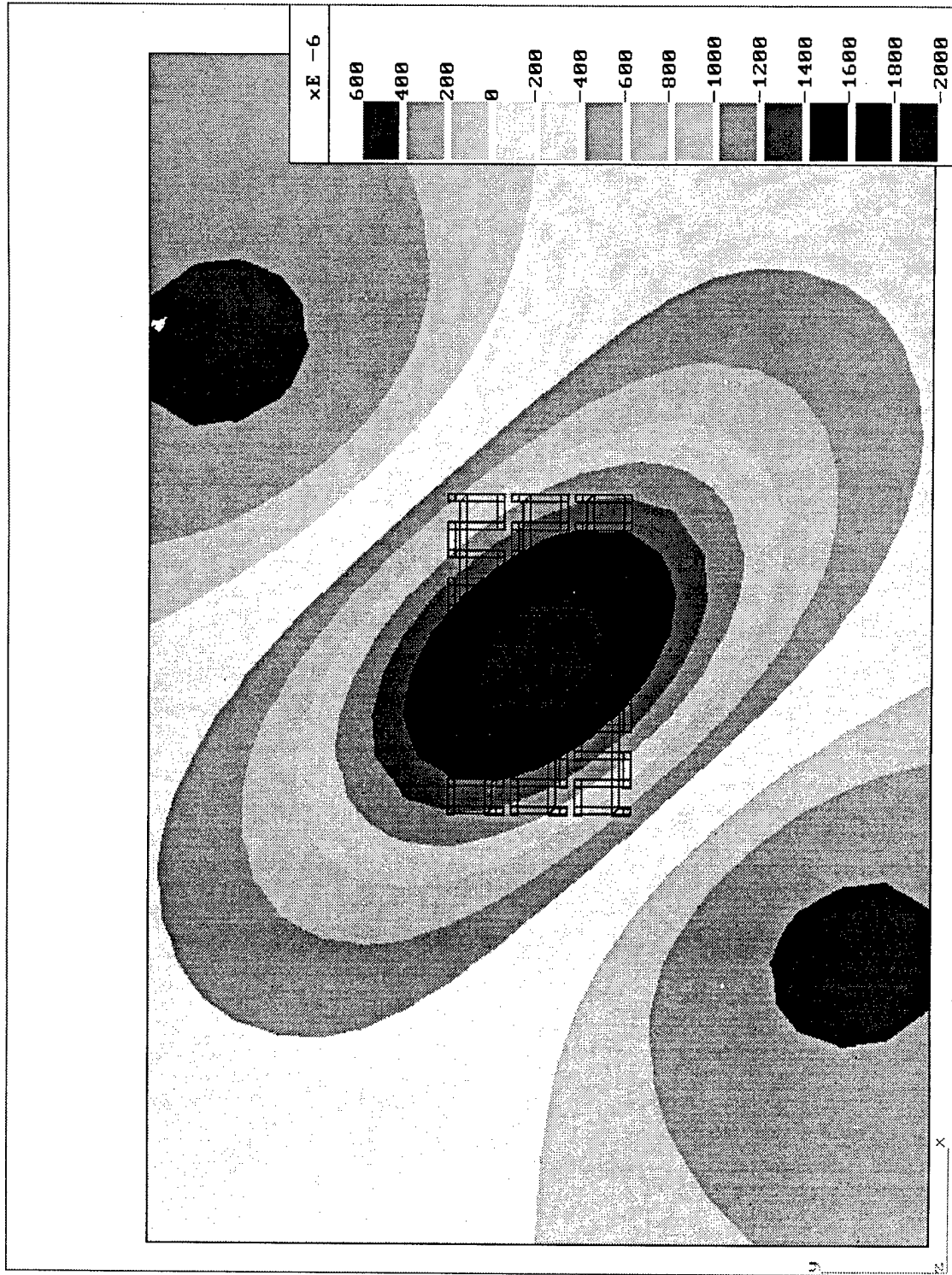*Figure 28. Geometry of numerical model for present configuration*

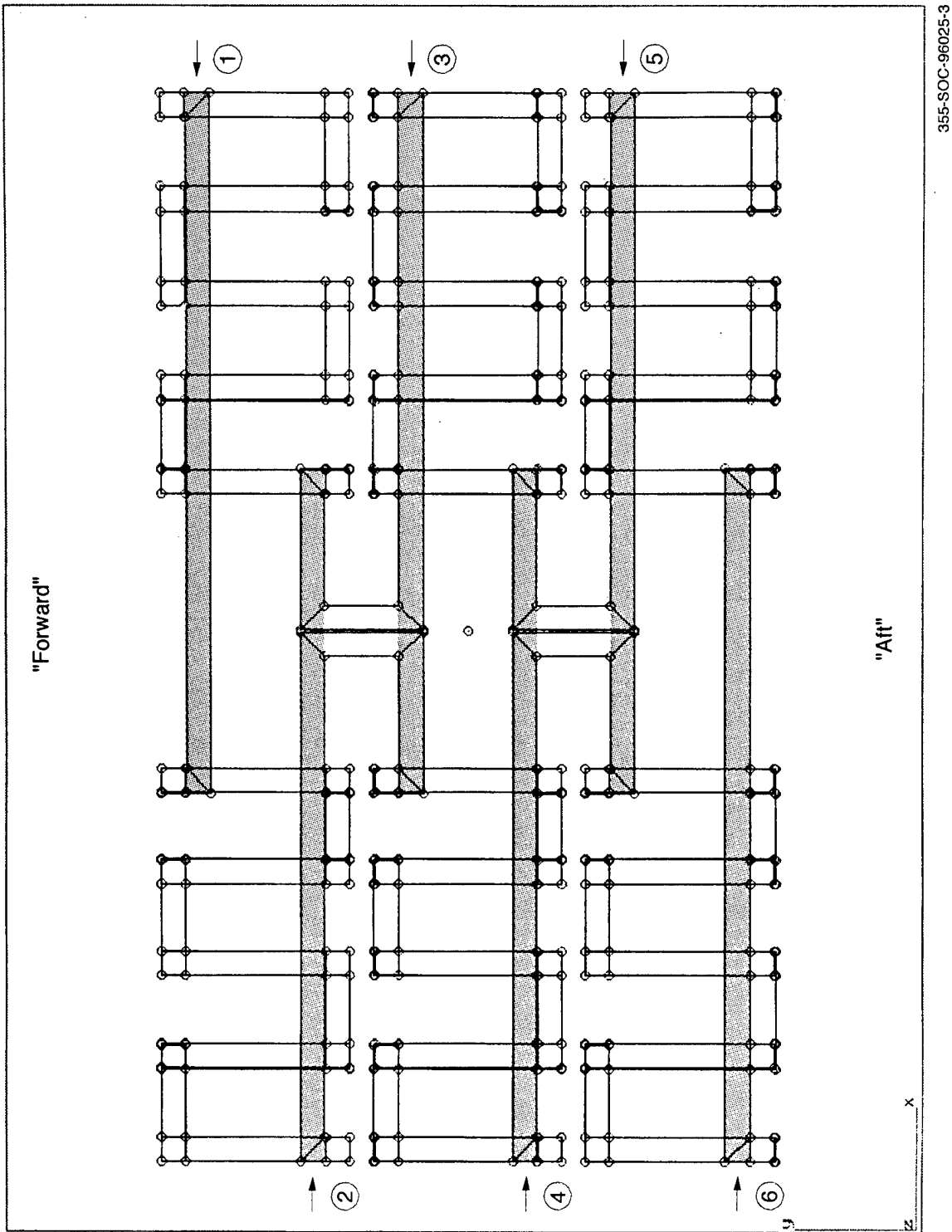**Figure 29.** *Vertical field contour plot for present configuration at 1m*

45

Figure 30. Slightly-modified present configuration numerical model
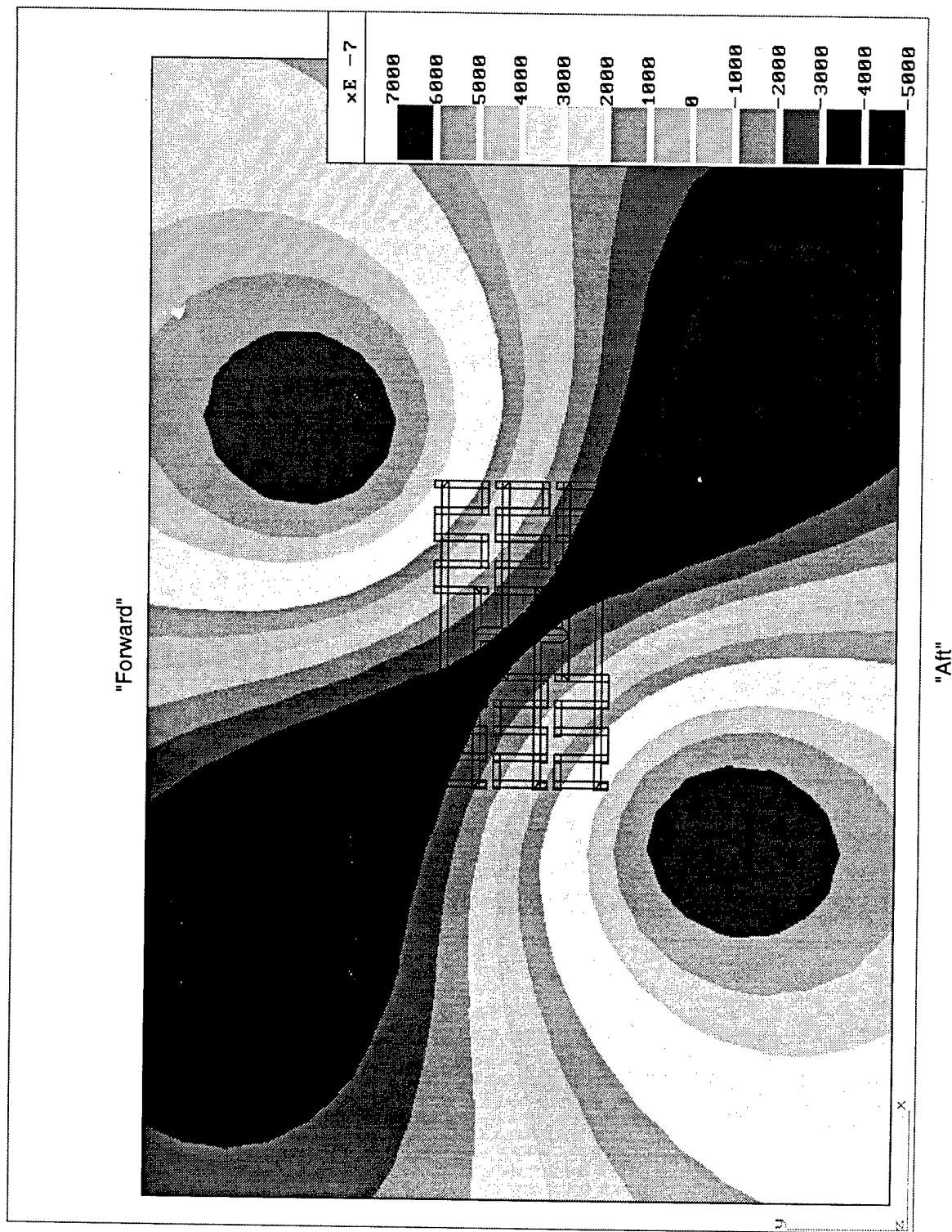
46

Figure 31. Vertical field contour plot for slightly-modified present configuration at 1m
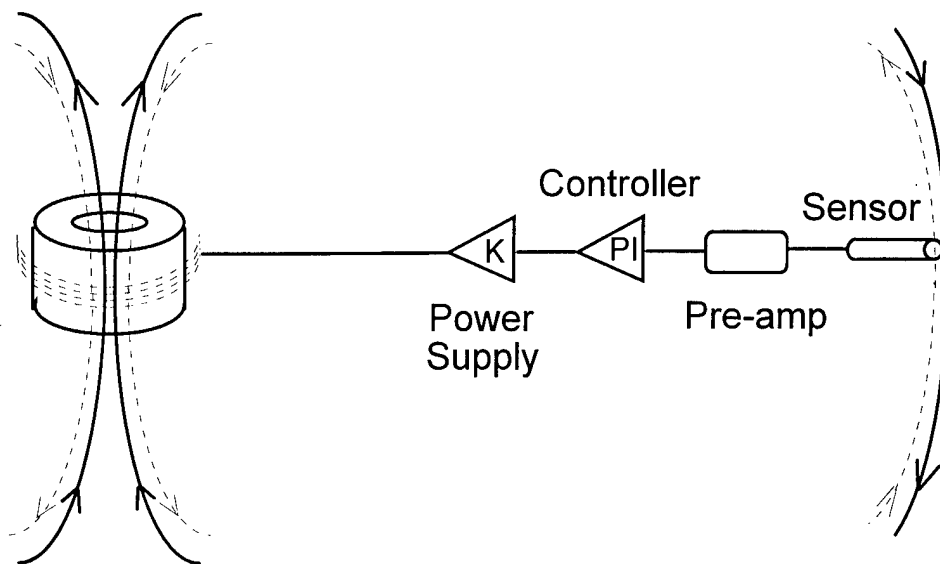
47

Figure 32. Conceptual active control scheme

controls current through a cancellation coil. The coil produces a magnetic field equal and opposite to the original source field resulting in zero net field at the sensor. In practice, the zero net field is actually biased to earth's field by a reference sensor. Figure 33 shows an artist's conception of an active cancellation system.

Through intelligent placement and orientation of the sensors and cancellation coils, the three components of the magnetic dipole can be de-coupled. This permits each coil to be driven with the appropriate current level independently. In this demonstration, the vertical (y) component of the magnetic dipole moment is controlled by the active control loop.

The active control loop used for magnetic field cancellation (for the y-oriented coil) is presented in Figure 34.

The active control system had a stationary three-axis magnetic field sensor placed beneath the induction motor to monitor the magnetic field in the immediate vicinity of the motor. This sensor monitored the magnetic field component along the three Cartesian axes. For reference purposes, the y-axis was vertical, the z-axis was aligned with the axis of motor rotation, and the x-axis is transverse to the motor axis and the vertical. A second magnetometer was positioned further away from the motor to monitor the ambient or reference magnetic field. When the motor shield was activated, an electronic circuit monitored the signal associated with the vertical (y) axis measurement near the motor, subtracted out the background magnetic field and amplified the difference using a high gain amplifier. This signal was then used to drive a power supply which injected current into a coil producing a vertical field wound around the motor (providing negative feedback). The coils producing fields along the other (x and z) axes were manually controlled. In an actual shield these coils would be automatically controlled precisely as the vertical field coil.

Motor

Perturbed
Magnetic Field

Magnetic Field
Sensor

z ←
y

Current
Drive

Amp

Differential
Circuit

Background
Magnetic Field

Reference
Sensor

349-SOC-96059-1
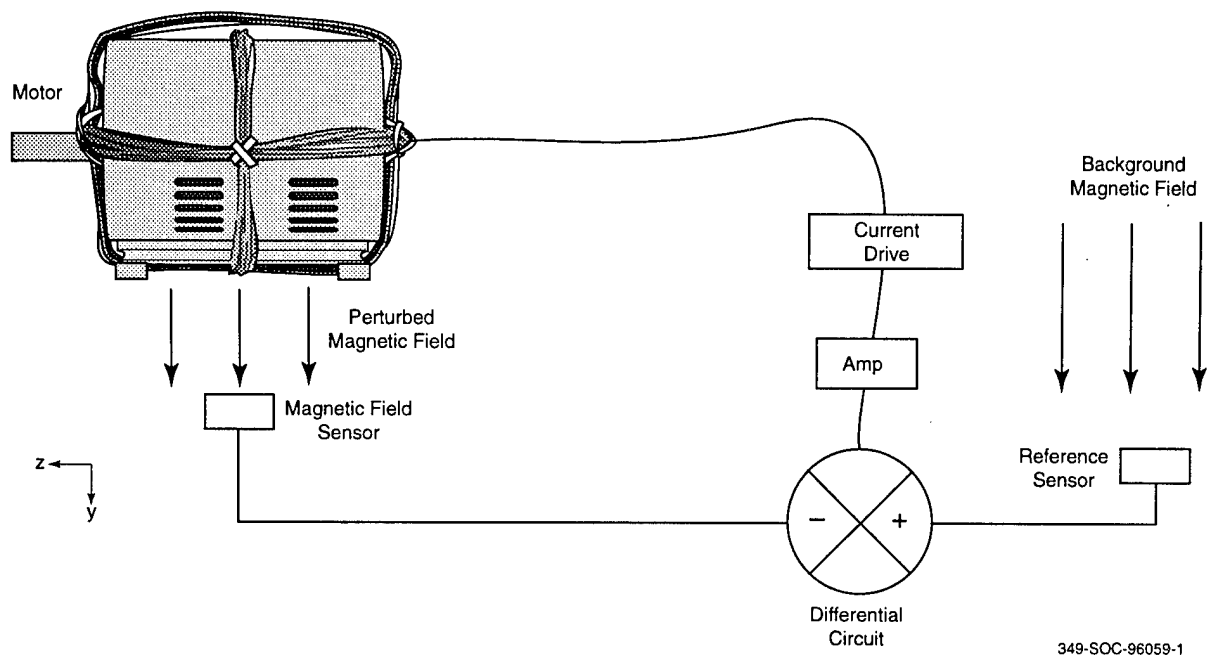
Figure 33.   Active control system for vertical axis coil

Motor
Field

Net Field

+

−

Coil

Power
Supply

Controller

+

Magnetometer
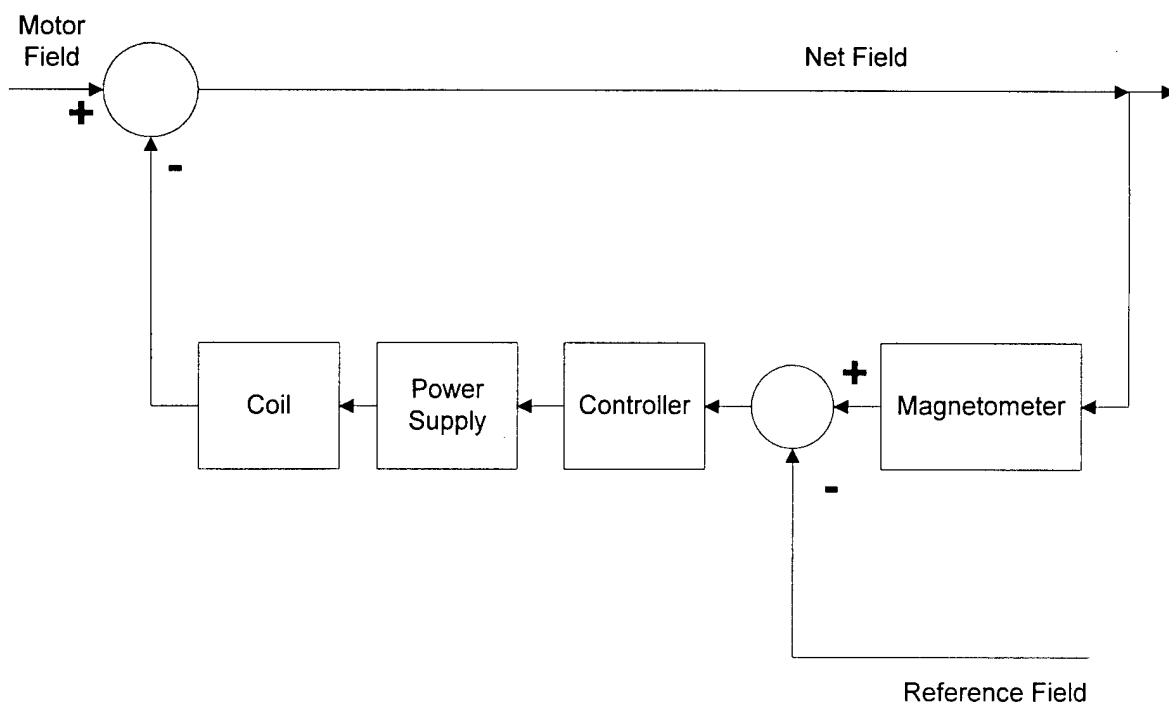
−

Reference Field

Figure 34.   Active control loop

49

When the sensor and coils are oriented properly, the magnetic field in the presence of the motor will be equal to the ambient or reference magnetic field.

The successful operation of the magnetic signature reduction system was demonstrated by moving a third magnetometer past the motor along a track aligned with the z-axis (aligned with the motor rotation axis). As the magnetometer array passed the motor, the three components of the magnetic field (B_x, B_y, B_z) were monitored and compared to those obtained in the absence of the motor.

A schematic diagram of this arrangement is presented in Figure 35.

6.3   Results of Active Magnetic Cancellation

The active control circuitry was engaged in order to demonstrate magnetic signature reduction. When the control circuitry and current drivers were activated, the results presented in Figure 36, Figure 37, and Figure 38 were obtained. Due to the complexity of the curves, each component of magnetic field will be presented separately.

The measured perturbation to the x component of the magnetic field was small due to the position of the motor and the orientation of the magnetometer array. This component of the field is presented in Figure 36.

As can be seen in Figure 36, the perturbation to the ambient magnetic field is less than the natural variations in the ambient field. Nevertheless, this perturbation must be canceled.

The y component of the magnetic field is equal to the vertical flux pointing directly out of the "North Pole" of the magnetic dipole. This field component has a single lobe which is maximized directly above the anomaly.
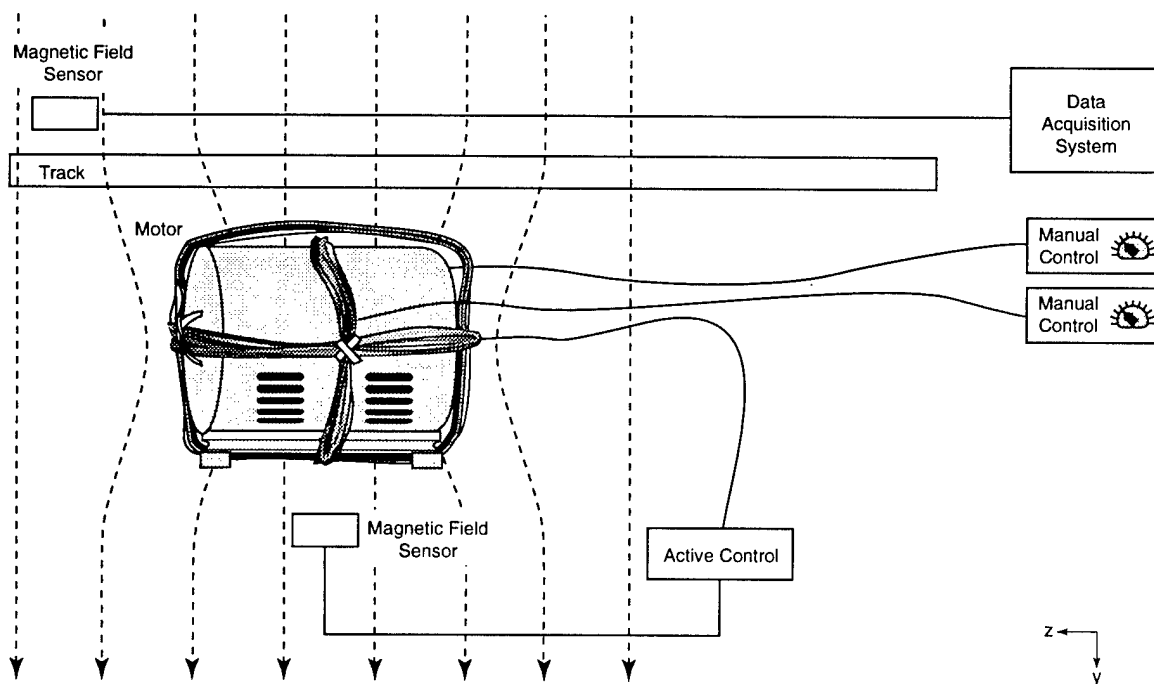

349-SOC-96059-2

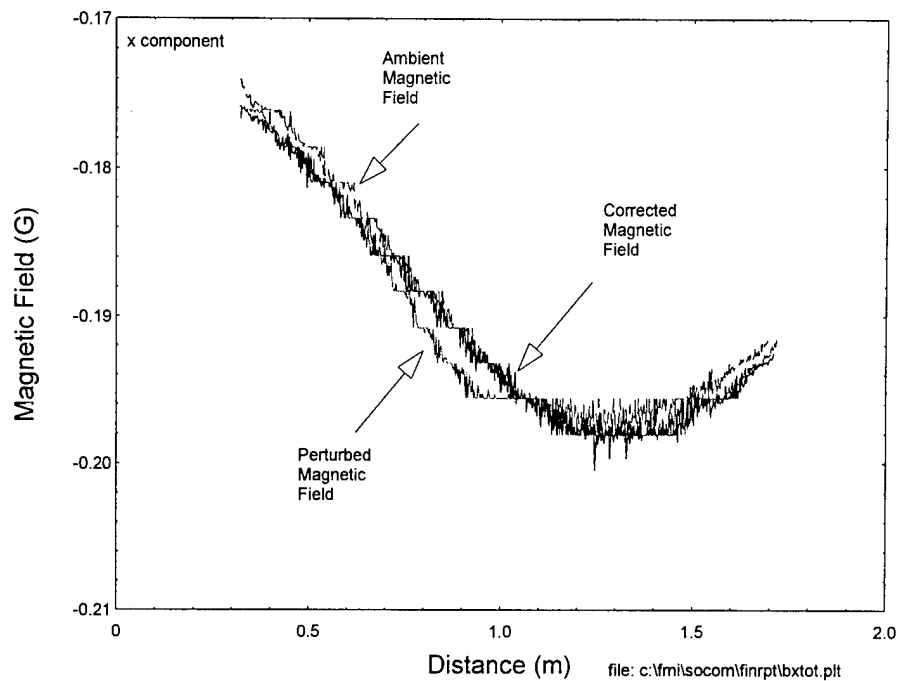*Figure 35. Experimental arrangement for magnetic signature reduction*

50

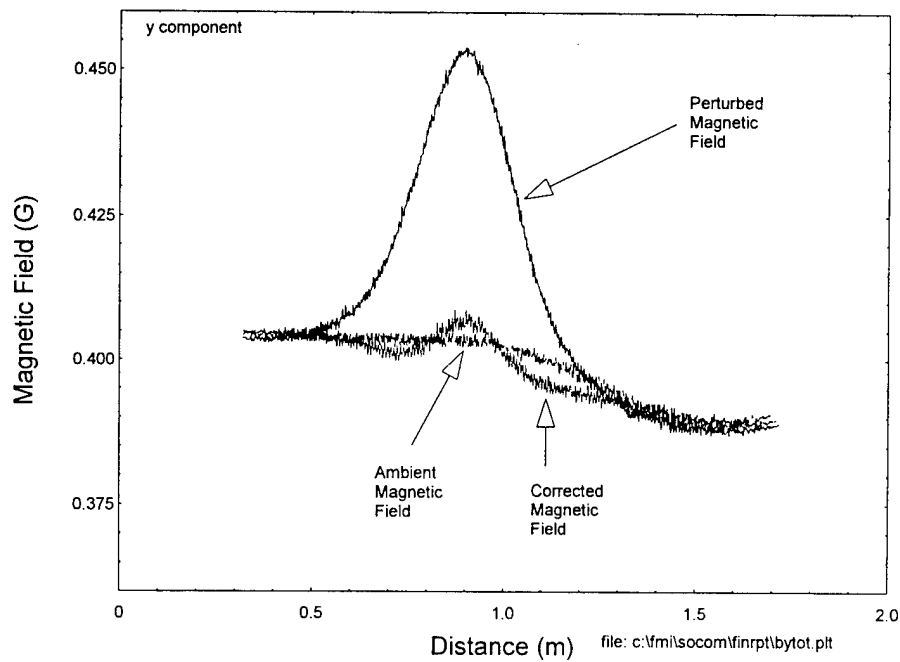**Figure 36.   Corrected x component of magnetic field**

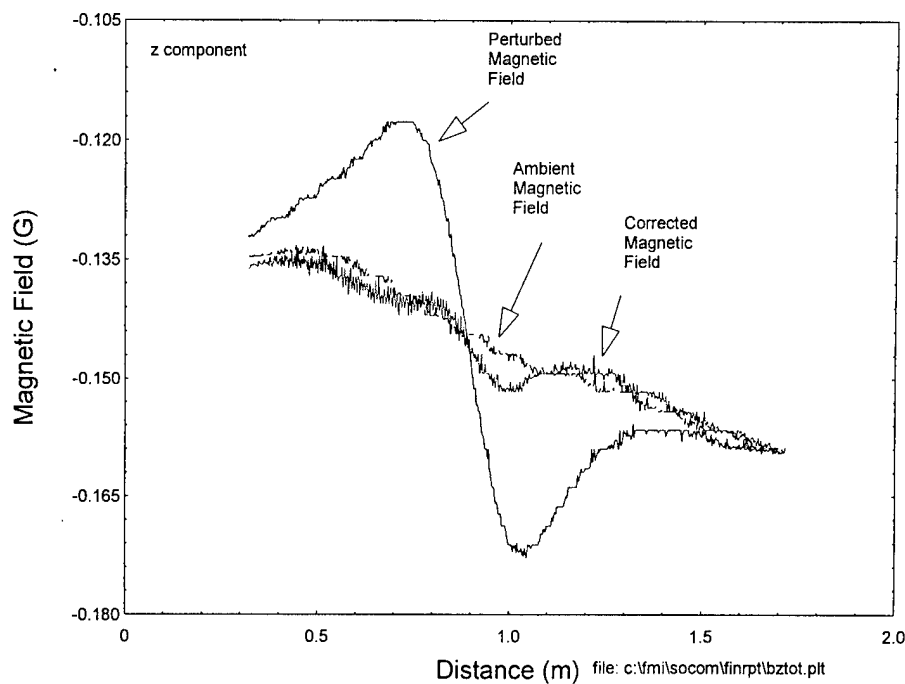**Figure 37.   Corrected y component of magnetic field**

Figure 38. Corrected z component of magnetic field

The small perturbations to the ambient magnetic field still remaining after correction are evidence of higher order poles in the magnetic field perturbations. This is due to the simple geometry chosen for the coil windings around the electric motor, as shown in Figure 5 (coils tightly wound together). These higher order moments can be reduced through the proper shaping of the cancellation coils wound around the motor.

When the perturbations observed in the corrected magnetic field are compared to those of the uncorrected magnetic field, the results presented in Figure 39 are obtained.

Figure 39 demonstrates the effectiveness of the magnetic signature reduction system. Note that these perturbation are graphed on the same scale axes. When the vertical scale is expanded for quantitative evaluation, the results presented in Figure 40 are obtained.

This graph demonstrates a 21 dB (>10:1) reduction in magnetic field perturbation when the field levels are compared to those obtained in the presence of the electric motor without the magnetic signature reduction system.

As discussed before, matching the multipole field characteristics of the cancellation field with the multipole field characteristics of the magnetic anomaly should lead to much higher levels of magnetic signature cancellation.

Active magnetic field cancellation can reduce this perturbation magnetic field through the creation of an equal, but opposite magnetic field: thus, restoring the net magnetic field levels to its ambient levels.

It is of interest, even at this early stage, to estimate the system impact of the active magnetic shielding subsystem. The parameters are provided in Table 4. Of course, significant
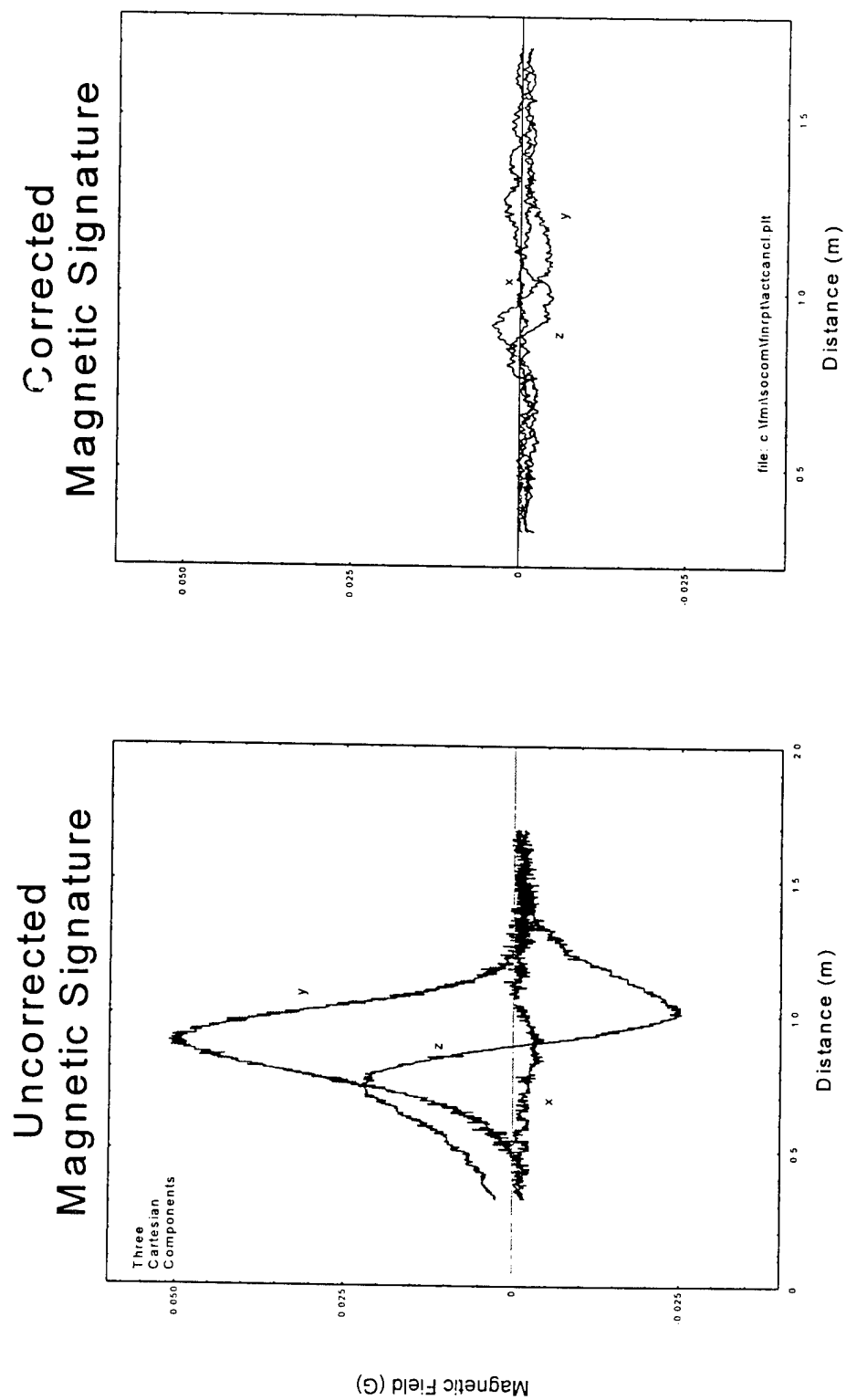
52

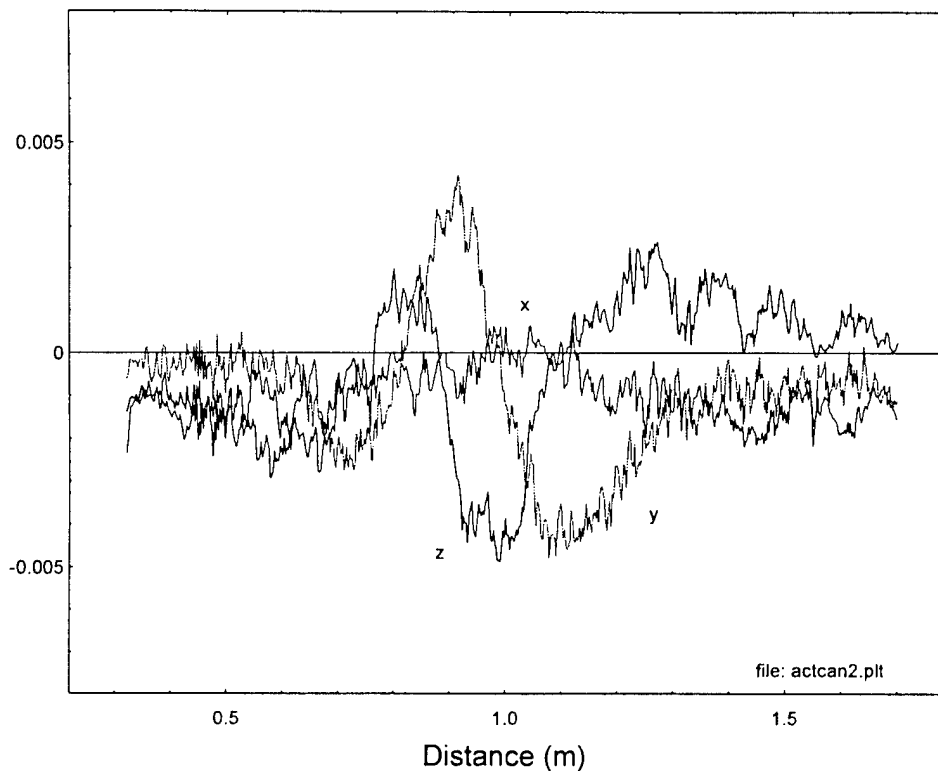*Figure 39. Uncorrected and corrected magnetic field perturbations*

Figure 40. Corrected magnetic field perturbations

Table 4. Technical data summary of motor active magnetic shield

Parameter	Estimated Value
Reduction in Magnetic Field	21 dB
Active Coil Size	10 in. diam x 1/4 in^2 cross section
Weight	Coil: 1 lb per axis
	Power Supply: 3 lb
Peak Voltage	5V
Peak Current	10A
Peak Power	50W

additional shielding development effort is necessary to actually implement the shield. Therefore, this table is provided simply to indicate that a minor system impact is anticipated for the active shielding subsystem.

6.4 Summary

In summary, a 21 dB reduction (>10:1) in magnetic signature reduction was experimentally obtained through active magnetic cancellation. This level of reduction was limited by the inappropriate bunching of the cancellation coils, leading to the presence of higher order multipoles in the magnetic cancellation field. The shape of the coil windings can be optimized through a detailed analysis of the anomaly multipoles.

The system impact of the active shield has been evaluated and is expected to be minor. Further shield development is certainly necessary but this conclusion is expected to be unchanged.

54

7. CONCLUSIONS

This section summarizes the overall approach taken during this program, and briefly reviews the results achieved. Because the technology is quite general, several other interesting applications of it are mentioned.

7.1   Methodology Summary

The methodology used during this program was one of measurements of the SDV magnetic field to define the problem; design and analyses to determine the best shielding configuration based upon the measurements, typically decomposing the field into its constituent parts in a manner similar to Fourier analysis of time waveform signals; and actual testing and validation of the shield design. Due to limited availability of the SDV a substitute motor was used in our laboratory and numerical calculations were made of the fields of the battery pack.

7.2   Magnetic Signature Reduction Achieved

The reduction in magnetic field is significant indeed. Measurements of the vehicle showed there were three main contributions to the emitted magnetic field.

- Magnetic material in the motor.
- Operation of the motor.
- Battery currents used to drive the motor.

Using the methodology discussed above, the results obtained were:

- Motor was shielded by -21 dB (a factor of approximately 10:1).
- Battery currents were shielded by -15 dB (factor of 5.7:1).

7.3   Other Applications

This methodology has been developed and used on several previous and ongoing projects. The past projects included:

- Magnetic field reduction of internal combustion engine.
- Solenoid-operated circuit breaker on mine countermeasure (MCM) ship.
- Interior and exterior of electric vehicle.
- Interior of maglev vehicle with superconducting magnets.

In addition, the methodology is being extended to other applications such as:

- Magnetic signature reduction of motor controllers (program in progress).

- Acoustic quieting of air ducts (program in progress).

- Acoustic quieting of the electric propulsion system (potentially included in Phase II of this project).

7.4   Summary

The test for robustness of a development methodology is its general applicability and the specific results achieved. We have demonstrated a significant reduction in magnetic field signature of SDV-like components based upon a well-proven signature reduction methodology. The results indicate magnetic field suppression of 15 to 21 dB for the two major contributors to the SDV magnetic signature. The capability exists to further reduce the signature using the same methodology with more time and resources spent with an actual SDV. The technology is being extended to include acoustic quieting as well as magnetic signature suppression.

8. RECOMMENDATIONS FOR PHASE II

Magnetic shielding feasibility was demonstrated for the SDV during this program. However, much work remains to be done before a fieldable system is retrofitted to a vehicle. This section briefly discusses the work that needs to be done and sketches the manner by which it will be accomplished.

There are two reasons for extending this work into a Phase II effort. The first reason is to obtain more realistic SDV operating conditions. This includes motor loading and shielding the actual motor and battery packs instead of a substitute motor and numerical model of the battery pack. The second reason is to develop further the actual shielding system including design and system integration.

8.1   Real World Operating Conditions

The most significant unexplored aspect of the magnetic signature of the SDV is that it is totally unmeasured under motor load. In the discussions above several mentions have been made concerning how the magnetic field increases with load. Therefore, one of the most important issues is to measure the signature under load. There is low technical risk associated with successfully accomplishing this task but it is very important to the overall reduction in emitted magnetic field as it impacts the battery pack fields and may impact the motor fields.

The next phase of the program should shield the actual motor used for the SDV. The present phase shielded a substitute motor since no SDV production motors were available. Excellent shielding results were obtained with the substitute motor and are anticipated for the SDV permanent magnet motor. Nevertheless, the work has not been accomplished and represents a clear task for Phase II. There is low technical risk associated with successfully accomplishing this task since it has been achieved with the substitute motor.

During Phase II the battery pack should be measured and shielded. This phase was limited by the low no-load current used to measure the field of the battery pack. Therefore, a reduction in field was demonstrated numerically but the more important point was the sensitivity of the field to the exact placement of the conductors. Hence, the field of the battery pack needs to be experimentally recorded at an increased battery current and the magnetic field of the battery pack should be measured as various conductors are slightly displaced. In addition, the battery pack conductors should be adjusted and secured to minimize the amount of stray field emitted. There is also low technical risk with this task. Technically the task of measuring and shielding the battery pack is very low risk and we have previously accomplished similar tasks for the electric vehicle batteries and a resistor bank for a large (350 hp) dc motor controller.

8.2   Shielding System Design and Integration

The shielding system will need to be carefully designed and integrated from a systems viewpoint. This will include additional measurements, as discussed above, shielding system and interface design, testing, validation, hardened packaging and operator interface and training considerations.

The logical sequence of individual tasks has been proven on previous magnetic signature reduction programs such as the NSWC mine countermeasures (MCM) ship solenoid-activated circuit breaker and the (land) electric vehicle shielding development for an Army TACOM/ Chrysler Corp. dual-use program.

8.3   Summary

In conclusion, a Phase II effort is recommended to further investigate and reduce the stray emitted magnet field of the SDV. There are two fundamental reasons for this recommendation:

- Measure the stray field of the SDV under more realistic conditions.
- Develop further and system integrate the magnetic shielding system.

The technical approach to accomplishing this goal has been proven successful previously in several related applications (NSWC MCM circuit breaker and TACOM/Chrysler electric vehicle) and there is low risk associated with successfully accomplishing a significant reduction in magnetic signature of the SDV.

9. REFERENCES

1. R.J. Thome and J.A.M. Tarrh, *MHD and Fusion Magnets, Field and Force Design Concepts*, Wiley, New York, 1982, p. 314.
2. Abramowitz, M., and I.A., Stegun, *Handbook of Mathematical Functions*, Dover, NY, 1972.
3. S. Ramo, J.R. Whinnery, and T.Van Duzer, *Field and Waves in Communications Electronics*, Wiley, 1984, p. 318 ff.
4. Jan Tuma, *Handbook of Numerical Calculations in Engineering*, McGraw-Hill, New York, 1989, p. 227.